ISSN 0973-3302

THE JOURNAL OF ACOUSTICAL SOCIETY OF INDIA

Volume 46 Number 1 January 2019

A Quarterly Publication of the ASI
http://www.acousticsindia.org

The Journal of Acoustical Society of India

Volume 46 Number 1 January 2019 pp 1-50

The Journal of Acoustical Society of India

The Refereed Journal of the Acoustical Society of India (JASI)

The Journal of Acoustical Society of India is a refereed journal of the Acoustical Society of India **(ASI)**. The **ASI** is a non-profit national society founded in 31st July, 1971. The primary objective of the society is to advance the science of acoustics by creating an organization that is responsive to the needs of scientists and engineers concerned with acoustics problems all around the world.

Manuscripts of articles, technical notes and letter to the editor should be submitted to the Chief Editor. Copies of articles on specific topics listed above should also be submitted to the respective Associate Scientific Editor. Manuscripts are refereed by at least two referees and are reviewed by Publication Committee (all editors) before acceptance. On acceptance, revised articles with the text and figures scanned as separate files on a diskette should be submitted to the Editor by express mail. Manuscripts of articles must be prepared in strict accordance with the author instructions.

All information concerning subscription, new books, journals, conferences, etc. should be submitted to Chief Editor:

B. Chakraborty, CSIR - National Institute of Oceanography, Dona Paula, Goa-403 004,
Tel: +91.832.2450.318, Fax: +91.832.2450.602, e-mail: bishwajit@nio.org

Annual subscription price including mail postage is Rs. 2500/= for institutions, companies and libraries and Rs. 2500/= for individuals who are not **ASI** members. The Journal of Acoustical Society of India will be sent to **ASI** members free of any extra charge. Requests for specimen copies and claims for missing issues as well as address changes should be sent to the Editorial Office:

ASI Secretariat, C/o Acoustics, Ultrasonics & Vibration Section, CSIR-National Physical Laboratory, Dr. KS Krishnan Road, New Delhi 110 012, Tel: +91.11.4560.8317, Fax: +91.11.4560.9310, e-mail: asisecretariat.india@gmail.com

ISSN 0973-3302

Printed at Alpha Printers, WZ-35/C, Naraina, Near Ring Road, New Delhi-110028 Tel.: 9810804196. JASI is sent to ASI members free of charge.

ASI

The Journal of Acoustical Society of India

A quarterly publication of the Acoustical Society of India

Volume 46, Number 1, January 2019

ARTICLES

INFORMATION

EDITORIAL

In the emerging new era, high-frequency acoustics plays a crucial role in the use of sensors and communications for Anti-Submarine Warfare (ASW) and Autonomous Undersea Vehicles (AUVs). Two of the most technologically advanced high frequency problems for navy are the underwater acoustic communications and design and development of synthetic aperture sonar (SAS). Presently, the researchers mostly focus on the dense signal processing rather in understanding the fundamental acoustics. The long range and high data rate drive the selection of frequency, bandwidth and power for an underwater acoustic communications system. However, in most of the practical cases, the desired data rates and ranges may or may not be well-suited because of the effects of multi-path, fading and Doppler. This leads to a compromise between what is feasible and what is really required. In some cases, utilizing different powers and frequencies for multiple mode of communication, the required data rates for these frequencies are achieved. Another field where the high frequency utilized by navy is in the mine hunting. To distinguish mines from other objects at the sea bottom and to obtain finer shape information of the object, large swath width and fine resolution is very much essential. Combining the AUV and SAS technology, the high frequency acoustics provide better concept for sensing and communications. Even though, the concept of SASis in the conceptual stage, it is an exciting application of high frequency acoustics. In spite of all these applications, the research on high frequency acoustics is extremely sparse in Indian scenario, which may be due to the lack sufficient high frequency acoustics data. Therefore, to highlight the importance of high frequency acoustics, a special issue of Journal of Acoustic Society of India with its Theme "High Frequency Acoustics" is planned.

Thespecial issueincludes six papers dealingdifferent aspects of high frequency acoustics. The papers are (i) Design and Development of high frequency transducer for underwater acoustic imaging by G Suresh, A. Shanavas and T Mukundan, (ii) Battery operated power amplifier for underwater sensor networks by Panchalai VN, Yateesh Kumar Mishra and Jeffin George, (iii) Ethernet and high voltage DC over single core coaxial cable for high frequency applications by Manoj G, Sona O Kundukulam, Biju Gopal and Unikkat Ganesan, (iii) A Study of Attenuation of Underwater Acoustic Signal in Shallow Water Environment by RP Raju, (iv) Effect of multipath arrival structure on temporal coherence of high frequency broadband transmissions in shallow water by Sreeram Radhakrishnan, Anilkumar K and Elizabeth Shani, and (vi) Transmission loss variability associated with high frequency internal waves in the Indian coastal waters by Anilkumar K, Sreeram Radhakrishnan, PV Hareesh Kumar.

The Guest Editor thanks Shri. S Vijayan Pillai, Director, NPOL for his encouragement to complete this special issue of JASI. He also thanks Dr. Biswajith Chakraborti, Chief Editor JASI for his consent and advice to consolidate the special issue.

Dr. PV Hareesh Kumar
Director (S&T) & Sc. G
NPOL, Kochi
Guest Editor

एस विजयन पिल्लई
उत्कृष्ट वैज्ञानिक
निदेशक
S Vijayan Pillai
Outstanding Scientist
Director

सत्यमेव जयते

भारत सरकार - रक्षा मंत्रालय
रक्षा अनुसंधान तथा विकास संगठन
नौसेना भौतिक तथा समुद्रविज्ञान प्रयोगशाला
तृक्काकरा, कोच्चि - 682 021
Government of India, Ministry of Defence
Defence Research & Development Organisation
NAVAL PHYSICAL & OCEANOGRAPHIC LABORATORY
Thrikkakara, Kochi – 682 021

FOREWORD

High-frequency acoustic sensing systems are typically preferred to low-frequency systems for the detection and classification of objects as they provide finer spatial as well as temporal resolution. However, the high frequency acoustic signals are subject to fluctuations depending on a combination of factors such as sea surface waves, depth and slope of thermocline, turbulence from internal waves, tides and currents. The amplitude and phase of such high frequency acoustic signals vary in response to changes in oceanographic conditions, imposing limitations on the exploitation of coherent signal structure.

As the area of interest shifts from the deep ocean towards the littoral waters, environmental influences become dominant both in time and space. A comprehensive analysis of the effects of the shallow water environment on the propagation of high frequency acoustic signals is needed to optimize sonar signal processing structures, for wideband signal and processor design, and for modeling acoustic propagation. The fluctuations in the coherent structure of the propagating signals impose limits on sonar system performance which then require compensation by appropriate signal processing techniques.

For high frequency applications, time spreading measurements can provide a measure of the acoustic bandwidth that can be transmitted in the unden/vater channel which can be used not only to improve performance predictions of existing sonars but also to aid in the design of future prototypes.

I place on record my appreciation to the editorial team of JASI for bringing out a special issue to address and document the recent advancements in this critical but specialized area of research and development. Each article in this special issue themed "High Frequency Acoustics" is intended to be a stand-alone advanced contribution to the field and summarizes the recent progress in the area of high frequency underwater acoustic experiments and modeling.

Before I conclude, I wish to thank the editorial board for their time and effort to review the papers and for assisting each author with their suggestions and encouragement.

S. Vijayan Pillai
Outstanding Scientist
Director

Phone: Off: 0484 – 2424878, Res: 2108763; Fax: 0484 – 2424858; email:director@npol.drdo.in

The Journal of Acoustical Society of India : Vol. 46, No. 1, 2019 (pp. 1-9)

Transmission loss variability associated with high frequency internal waves in the Indian coastal waters

Anil Kumar K., Sreeram Radhakrishnan and P.V. Hareesh Kumar
Naval Physical and Oceanographic Laboratory, Thrikkakara, Kochi-682021
e-mail:anilnpol@gmail.com

[Received: 01-10-19; Revised: 05-11-19; Accepted: 11-11-19]

ABSTRACT

Fine resolution temperature and salinity data collected from the coastal waters of India along with an acoustic propagation model, Bellhop are utilized to study the high frequency internal wave (IW) characteristics and its influence on transmission loss variability. In the coastal waters off the southeastern Arabian Sea (SEAS), high frequency IWs of (~ 16 cph, 4 min) having amplitude of 8-12 m are noticed whereas in the northeastern Arabian Sea (NEAS), the corresponding values are ~ 28 cph (2.1 min) and 12 m respectively. The Andaman Sea also indicated the high frequency IW (~ 26 cph, 2.37 min) with amplitude of 8-14 m corresponding to the crest of the IWs. The presence of a strong thermocline sandwiched between upper and bottom isothermal layers, known as tri layer structure, favoured the formation of very high frequency IWs in this region. In all the cases, the amplitudes were found to vary with depth depending on the vertical estimate. The Acoustic propagation model, Bellop based on ray theory was utilised to estimated the transmission loss variability due to the high frequency IWs at all the three locations. These high frequency IWs caused a transmission loss variability of 15 dB, 22 dB and 18 dB in the SEAS, NEAS and Andaman Sea respectively. The TL was also found to amplify with increase in propogation ranges in the presence of IWs.

1. INTRODUCTION

Internal waves (IWs) are common in the coastal waters, where density stratification exists. These waves are generated by any disturbance caused in the density stratified water column, when a fluid displaced from its equilibrium level experiences a buoyant restoring force balancing the force of gravity. These waves are complex in nature with possible sources at surface (atmospheric forcing with wind stress and buoyancy fluxes) and bottom (tides and currents over rough topography). IWs occupy a vast range of spatial and temporal scales (Garret and Munk 1972, 1975), with horizontal scales ranging from few tens of meters to few kilometers and temporal scales from inertial to local Brunt-Vaiisala frequency, Nz. The particular type of IWs most frequently noticed in the ocean is termed a solitary waves or soliton. It can propagate very long distance without loss much its energy. Solitary waves are a class of nonsinusoidal, nonlinear, more-or-less isolated waves of complex shape. These internal solitons are generally composed of several oscillations (solitary wave packets) confined to a limited region of space (Apel, 2003). IWs with tidal periodicity are quite ubiquitous in the stratified waters over continental shelf (Craig, 1987). The interaction of IWs and mixing processes is a significant mechanism for nutrient transport and other biochemical processes (De Silva *et al.*, 1997; Nishri *et al.*, 2000). IWs has a profound influence on underwater acoustic propagation (Colosi *et al.*, 1998). These waves may break causing small scale turbulence (D'Asaro & Lien,

2000) and this combination has been found to have a substantial effect on arrival time fluctuations during short range propagation (Henyey *et al.*, 1997).

IWs are prominent in the Indian coastal and deep waters (LaFond 1961; Murty and Hareesh Kumar *et al.*, 1990; Sarma *et al.*, 1991; Hareesh Kumar *et al.*, 2006) and cause large fluctuations in the thermohaline fields. An insight into IWs in the seas around India has been broadly described by Murthy (2002). In the recent past some studies are carried on IWs in the seas around India utilizing the time series measurements from stationary ships and data from the oceanographic buoys in the Arabian Sea (Murthy and James, 1996; Murthy and Mohan Kumar, 1996; Krishna Kumar and Murthy, 1998, Hareesh Kumar, 2011). Transmission loss variability of 38.4 dB was reported at a coastal station off Paradeep in the presence of low frequency IWs (Sridevi *et al.*, 2011). Most of these studies dealt with the characteristics of low frequency IWs and their variability with space and time. However, a detailed study on transmission loss variability associated with high frequency IW characteristics are not carried out due to the sparcity of fine resolution field observations. Therefore, in this paper, the high frequency IW charcteristics in the Indian waters and associated transmission loss variability are addressed and analyzed.

2. DATA DESCRIPTION

Fine resolution time series measurements of temperature (5 sec intervals) were made from a shallow water, mooring deployed at the edge of the continental shelf (depth ~ 70 m) of the South Eastern Arabian Sea (SEAS) during March 2013 (1830 hrs on 5 March to 1800 hrs on 8 March). The vertical mooring consists of a 24 - channel thermistor array, with each sensors spaced at 2.5m. In addition, Conductivity-Temperature (CT) and depth sensors were also attached to the thermistor chain array to measure the density and depth variations. In addition, from an anchored ship, Conductivity-Temperature-Depth (CTD) data was also collected on hourly basis (total ~ 70 profiles) during the experiment to study the water column stratification. Another CTD data set used in this study is from the North Eastern Arabian Sea (NEAS) sampled at 5 min intervals during 1-3 November 2000 for a duration of 48 hrs (water column depth is 50 m). The third location considered in this study is the Andaman Sea (depth ~50 m) where the CTD data was collected at 5 min intervals for a duration of 19 hrs.

The Tide Model Driver (TMD), a Matlab package for accessing the harmonic constituents and for making predictions of tide height and currents is utilised to extract the barotropic tide for different constituents of the time - series data. A propagation model based on ray theory, Bellhop (http:// oalib.hlsresearch.com/modes/acoustictoolbox/ at.zip) was utilised to compute transmission loss (TL) associated with the passage of high frequency IWs. TL is a quantitative measure of the reduction in sound intensity between the source and receiver.

$$TL = 10 \log_{10} (I_{ref}/I) \quad (1)$$

where Iref is the reference intensity, measured at a point 1m from the source to the intensity I, measured at a distant point and is expressed in units of decibles (dB). Acoustic model, Bellhop is designed in order to perform two dimensional acoustic ray tracing for a given sound speed profile c (z) or a given sound speed field c (r, z) in ocean wave guides with at or variable absorbing boundaries (Porter and Bucker, 1987; Jenson *et al.*, 1994).

3. RESULTS AND DISCUSSION

The fluctuations noticed in the temperature field can be regarded as proxies for the vertical displacements induced by the IWs (Colosi *et al.* 2001; Holloway, 1984). Based on the relation between density, temperature and salinity (Apel, 1987; Yang *et al.*, 2004) found that rate of change in temperature with depth is about an order of magnitude higher compared to the rate of change in salinity, which can be neglected and temperature alone can be considered as proxy for IWs studies. The vertical displacements are estimated using various methods such as relation between temperature fluctuations and background

temperature gradient (Apel *et al.* 1997), inverse mapping to convert temperature to vertical displcement (Rubenstein, 1999; Apel *et al.* 1997; Lynch *et al.* 1996), and depth offset of the isotherm from depth of mean temperature are found to be embedded on the low fequency IWs with tidal periodicity. The figure (Fig. 1B) shows maximum variability in temperature associated with the IWs with semi-diurnal tidal periodicity, which is clearly seen from the Tide data. Another noticeable observation is that the high frequency oscillations follow a non - linear pattern. For example, in the initial 24 hrs, rhythmic oscillations are noticed in thermocline with larger amplitude in the upper thermocline compared to its lower part (Fig. 1A). However, between 1845 hrs and 2245 hrs on 05 Mar 2013, high frequency fluctuations of the order of 8-12 m amplitudes are noticed between 22 m and 37.5 m depths at the crest of the IWs with tidal periodicity. Possibly this could be due to the disturbance caused by the strong winds (~12 m/s) prevailed in the study region during this period (Figure not presented). Similar trend is also noticed during 0200 hrs to 0300 hrs on 08 Mar 2013 between 20 m and 37.5 m and during 0945 hrs to 1545 hrs on 06 Mar 2013 in the depth ranges of 22.5 - 32.5 m. The amplitudes and depth of occurence of these high frequency IWs reduced during 0600 hrs on 6 March 2013 to 0600 hrs on 7 March 2013 (between 45-65m). This can be seen from the depth-time section of N (z) (Fig. 1C) which also suggest the occurrence of high frequency IWs (N is ~16 cph, *i.e.* ~4 min) during the initial period compared to the final stages of the observation program (N is 10 cph, *i.e.* 6 min).

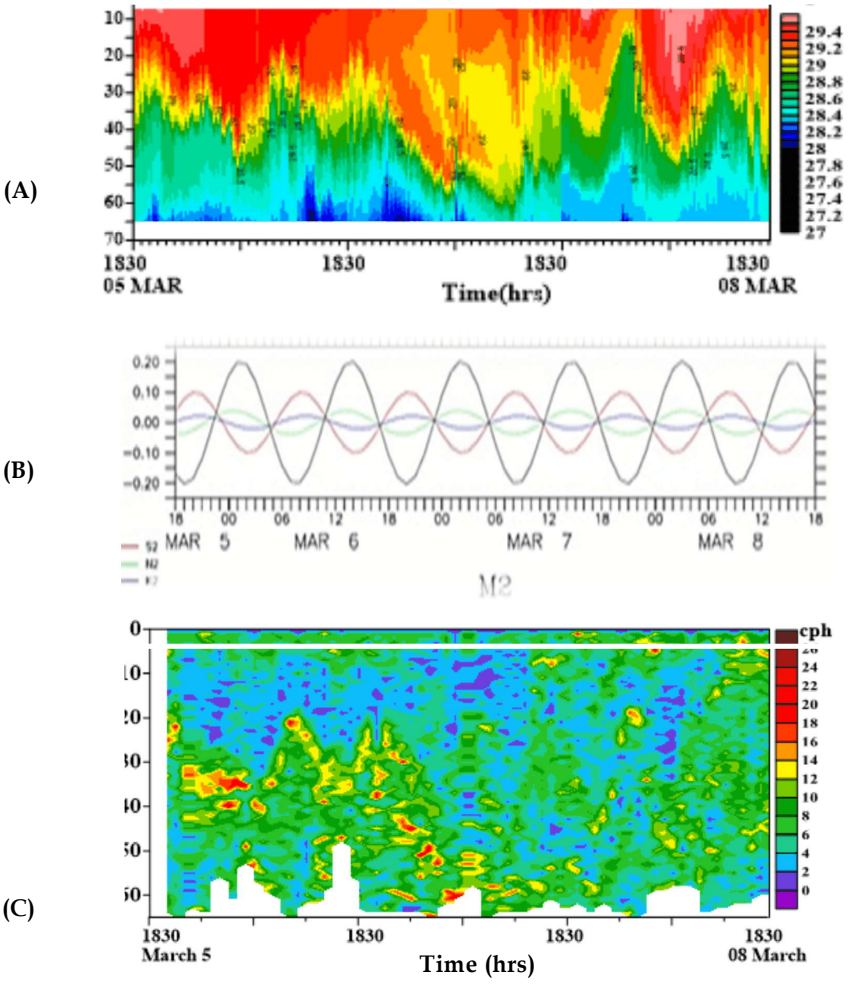

Fig. 1: (A) Vertical section of temperature (B) Corresponding barotropic tidal components (TMD) and (C) Brunt-Vaisala frequency, N(z) in the Southeastern Arabian Sea

3.1 IW characteristics in the Northeastern Arabian Sea

The vertical section of temperature in the North Eastern Arabian Sea (Fig. 2) during November shows surface (0-25 m) and bottom (25-45 m) homogeneous layers with a strong thermocline (3.52°C in 10 m) sandwiched in between. This type of structures are usually termed as the tri-layer structures. The strong vertical gradients in the thermocline is conducive for the formation of high frequency IWs. The figure shows high frequency IWs riding over the IWs with tidal periodicity with amplitude of 12 m at its crest. Vertical section of salinity indicate possession of Arabian Sea high salinity watermass (>36.5 psu) upto 35 m depth and strong salinity gradient (0.04 psu/m) between 35-45m. Depth-time section of N*(z)* suggest the existence of high frequency IWs (with maximum of 28 cph ~2.14 min and minimum of 16 cph ~ 4.28 min) in the thermocline centered at 35 m depth.

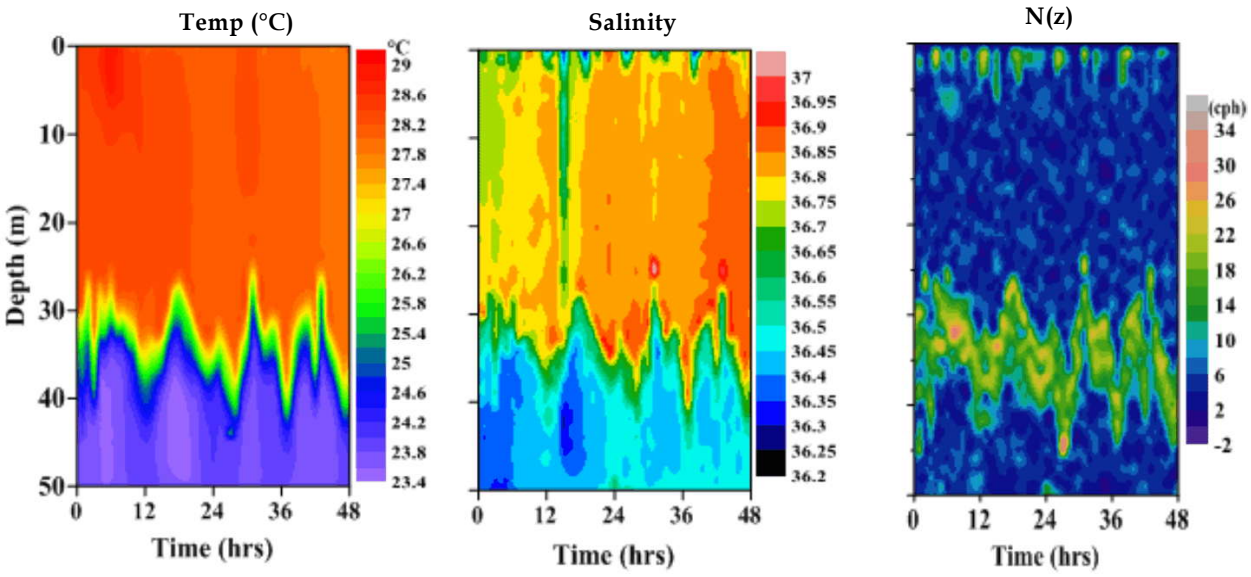

Fig. 2: Depth-time section of temperature, salinity and N*(z)*- Northeastern Arabin Sea

3.2 IW characteristics in the Andaman Sea

Andaman Sea is located along the eastern side of the Indian Ocean between Malaya Peninsula Andaman and Nicobar Islands. This region is prone to strong IWs activity with very large amplitude (> 60 m), wavelength (6-15 km) and speed (> 2.0 m/s) (Alpers *et.al.*, 1997). The large irregular bottom topography and salinity stratification leads to generation of enormous IWs in this region. Here, the depth-time section of temperature (Fig. 3) indicate weakly stratified waters in the upper 25 m (0.02°C/m) and relatively strong gradient (0.13°C/m) near the bottom (20-50m). Isotherm exhibits oscillation near the bottom stratified layers mainly due to the passage of IWs with semi-diurnal periodicity with amplitudes of the order of 8-14 m. The salinity section also exhibits similar type of oscillation. Here, the salinity shows minimum values (>32 psu) in the surface layers and it increases to bottom (33.7 psu) of the water column. The time evolution of N*(z)* also supports the generation of high frequency IWs (~ N is ~ 26 cph, 2.37 min) close to the bottom of the water column.

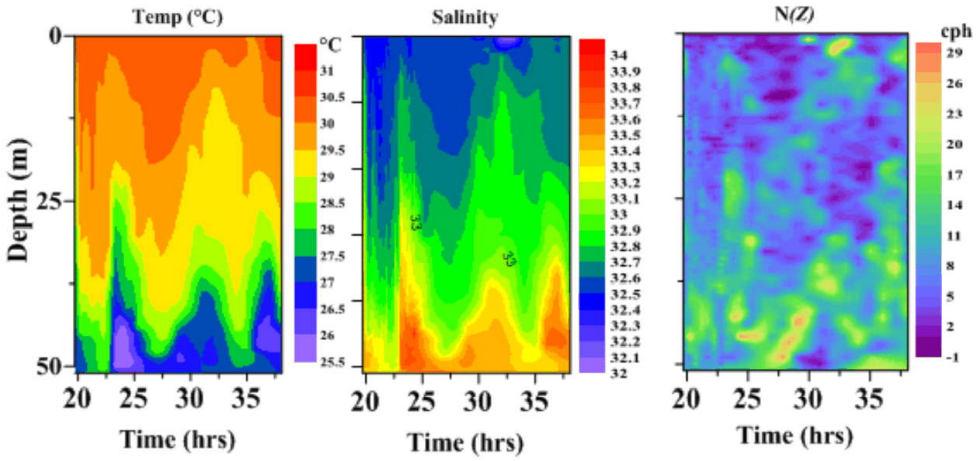

Fig. 3: Depth-time section of temperature and salinity and N(*z*) in the Andaman Sea

3.4 Transmission loss (TL) variability

The acoustic propagation model, Bellhop based on ray theory is utilised to estimate TL variability at all three stationary locations. This is achieved through utilising 25 sound speed profiles (from temperature and salinity data) corresponding to the crest of the IWs. The estimated TL values are extracted different ranges *viz.*, 1 km, 5 km, and 10 km for different times were utilized to generate the temporal variability of TL with respect to depth.

The coastal waters of the SEAS is characterized by weak thermal gradient during March and hence relatively weak sound speed gradient. With this prevailing stratification during the initial period, the periodicity of the high frequency IW is found to be ~ 4 min. As the stratification further weakens towards the end of observations, the periodicity increases to 6 min. Figure 4 (a), shows that that at a range of 1 km, a weak region of TL is found sandwiched between two TL maxima (>80 dB) close to the surface. The time gap between the occurrence of these two TL maxima is approximately 5 minutes, which is the periodicity of the high frequency IWs prevailed at this location during March, *i.e.* 4 minutes. These IWs cause a fluctuation

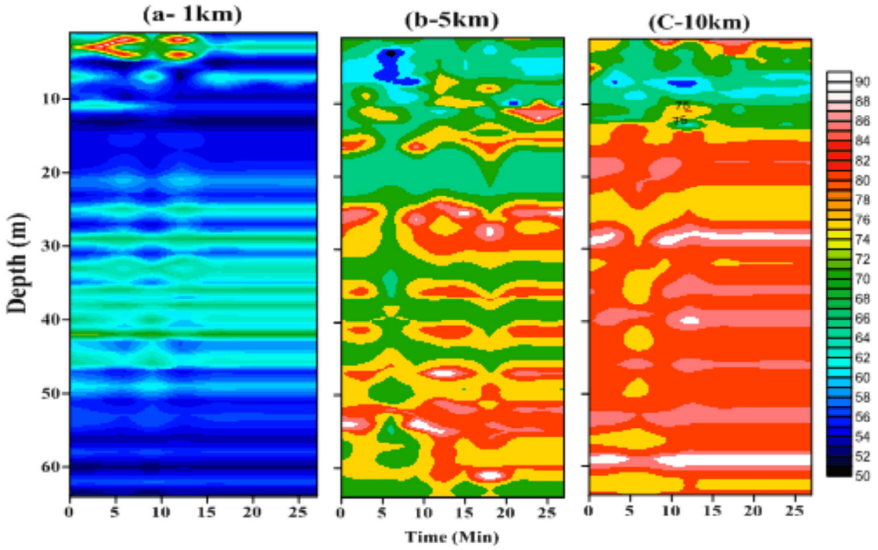

Fig. 4: Temporal evolution of TL at 1 km, 5 km and 10 km ranges from the source in the southeastern Arabian Sea

of ~10 dB in the TL at a distance of 1 km. Similar features, though weak is noticed during rest of the time because of the weak stratification and weak amplitude of the IWs. At the subsurface depths also, though there is significant reduction in the TL (<65 dB), alternate bands of comparatively high and low TL values, which corresponds to the periodicity of the IWs are seen. At a distance of 5 km (Fig. 4b), there is significant increase in TL in the entire water column, with TL values around 65 dB in the upper 25 m water column and in excess of 80 dB below this depth. In this case also, a temporal variability of ~10 dB is observed in the TL values corresponding to the passage of high frequency IWs. From Fig. 4c it is found that comparatively low TL (<65 dB) values in the upper layers and in excess of 85 dB below 25m indicating a difference of ~40 dB at 10 km ranges. In general, the role of high frequency IWs are significantly seen in the TL values for the three different ranges.

The acoustic propagation model is further utilised to study the influence of IWs on TL variability in a tri-layer scenario that prevailed in the North Eastern Arabian Sea during November. In this case also, sound speed profiles corresponding to the crest of the IWs are considered for the TL estimation. At a distance of 1 km, though TL is almost uniform in the entire water column (65-75 dB), alternate bands of low and high TL values close to the periodicity of high frequency IWs (~2 min) are observed. The TL exceeds 90 dB at a range of 5 km and further to 120 dB at 10 km range (Fig. 5 a, b, c). The influence of the high frequency IWs are very prominent at 5 and 10 km ranges than at 1 km. It is assumed that the presence of a strong thermocline as observed in the latest is responsible for these changes. Here, these waves caused a variability of nearly 50 dB both at 5 km and 10 km with maximum values noticed between 5 and 10 m depths. The results indicated that the input sound speed profiles exhibit strong gradient in the high frequency band due to the presence of IWs through out the water column.

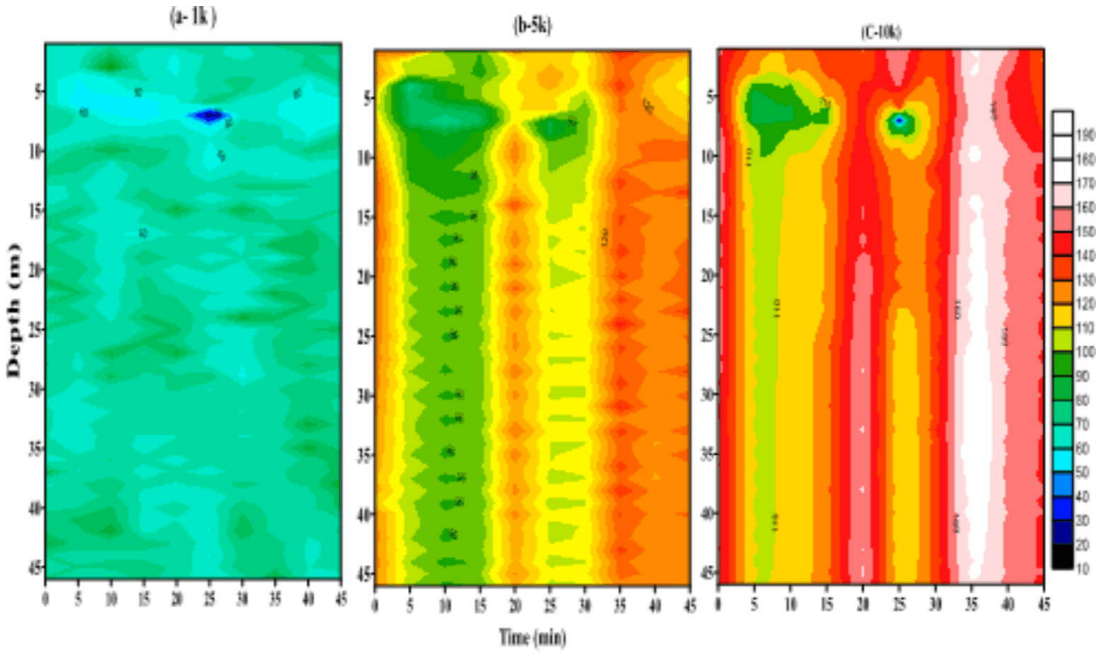

Fig. 5: Temporal evolution of TL due to high frequency IWs in the Northeastern Arabian Sea

In the Andaman Sea, temporal evolution of TL at 1 km, 5 km and 10 km ranges are presented in Fig.6. For 1 km range, the TL is more than 65 dB during the initial period up to 30 m depth and later reduces to 50-55 dB. In this case also alternate bands of weak and comparatively high TL values, coinciding with the periodicity of low frequency IWs are seen; the variability with time is relatively less (~5 dB) compared to the other two cases. At a range of 5 km, the TL increase to 105 dB during the initial period and reduces to 80 dB subsequently. The TL further increases to 100 dB at 10 km ranges and reduces to 75 dB after

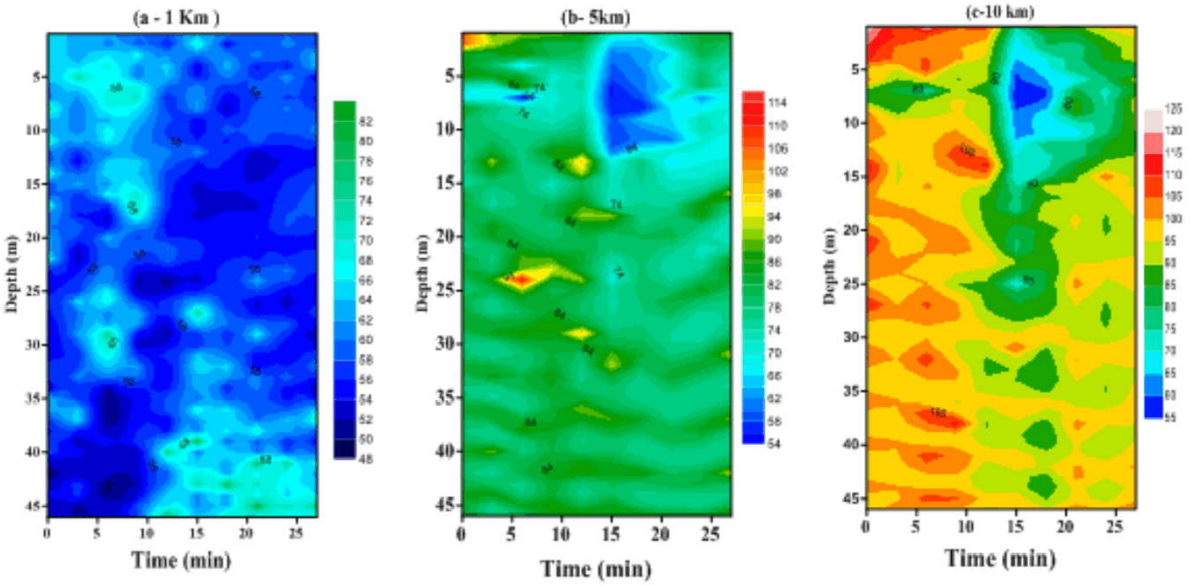

Fig. 6: Temporal evolution of TL due to high frequency IWs in the Andaman Sea

15 minutes. Near the bottom, where the water column is stratified, alternate bands of low and comparatively high values of TL with a time interval of 6-8 minutes (~20 dB variability in TL) is noticed.

4. CONCLUSION

Acoustic propagation in the ocean is influenced by many oceanographic features, among which the effect IWs is found to be the maximum. Utilizing high frequency temperature and salinity data coastal waters of northeastern Arabian Sea, southeastern Arabian Sea and Andaman Sea indicated prominent internal wave activity with different amplitudes for different frequencies. Though our study revealed both low and high frequency IWs, in the present case, we focused on high frequency IWs that are observed at the crest of low frequency IWs. The time evolution of transmission loss variability associated with these high frequency IWs are estimated using the ray based acoustic propagation model. As Expected, the study reveals increase in TL with ranges. The maximum variability in TL associated with the high frequency IWs (50 dB), is observed in the northeastern Arabian Sea during November. At the other two locations, the variability is around 20-30 dB and occurs at the stratified region of the profile. This study highlights the significance of high frequency IWs in the coastal regions of the Indian waters in the TL variability.

5. ACKNOWLEDGMENTS

Authors are thankful to Director, NPOL for providing necessary support and encouragement to carry out this work. Authors are also thanks commanding officers and crew and the participants for collecting the data for this study.

6. REFERENCES

[1] Apel J.R., 1987. *Principles of Ocean Physics* **38**. Academic Press.

[2] Apel J.R., 2003. A new analytical model for internal solitons in the ocean. *Journal of Physical Oceanography*, **33**(11), 2247-2269.

[3] Apel J.R., Badiey M., Chiu C.S., Finette S., Headrick R., Kemp J., Lynch J.F., Newhall A., Orr M.H., Pasewark B.H. and Tielbuerger D., 1997. An overview of the 1995 SWARM shallow-water internal wave acoustic scattering experiment. *IEEE Journal of Oceanic Engineering,* **22**(3), 465-500.

[4] Alpers W., Wang-Chen and Hock L., Observation of Internal waves In the Andaman Sea by ERS SAR, " Proc. 3rd ERS Symposium on Space at the service of our Environment, Florence Italy, 17-21 March, 1997, pp. 1287-1291.

[5] John A., Colosi., Michael G. and Brown., 1998. Efficient numerical simulation of stochastic internal-wave induced sound-speed perturbation fields, *Journal of Acoustic society America.* **103**(4), 2232.

[6] Craig P.D., 1987. Solutions for internal tidal generation over coastal topography. *Journal of Marine Research,* **45**(1), 83-105.

[7] D'Asaro E.A. and Lien R.C., 2000. The wave-turbulence transition for stratified flows. *Journal of Physical Oceanography,* **30**(7), 1669-1678.

[8] De Silva I.P.D., Imberger J. and Ivey G.N., 1997. Localized mixing due to a breaking internal wave ray at a sloping bottom. *Journal of Fluid Mechanics,* **350**, 1-27.

[9] Desaubies Y. and Gregg M.C., 1981. Reversible and irreversible fine structure. *Journal of Physical Oceanography,* **11**(4), 541-556.

[10] Garret CJR and Munk W.H., 1975. Space time scales of internal waves. A progress report. *J Geophys Res,* **80**, 291-297.

[11] Garret CJR and Munk W.H., 1972. Space time scales of internal waves. *Geophysical Fluid Dynamics* **3**, 225-264.

[12] Hareesh Kumar P.V., Sanilkumar K.V. and Panchalai V.N., 2006. Shallow water internal waves and associated acoustic intensity fluctuations. *Def. Sci. Journal,* **56**, 485-493.

[13] Hareesh Kumar P.V., A. Raghunadha Rao., Anilkumar, K., Padmanabham, M. and Radhakrishnan, K.G., 2011. Low frequency internal waves and their influence on transmission loss variability, *Nat. Hazards,* **57**, 643-656.

[14] Henyey F.S., Rouseff D., Grochocinski J.M., Reynolds S.A., Williams K.L. and Ewart T.E., 1997. Effects of internal waves and turbulence on a horizontal aperture sonar. *IEEE Journal of oceanic engineering,* **22**(2), 270-280.

[15] Krishna Kumar G.V. and Murthy P.G.K., 1998. Internal wave characteristics in the coastal waters off Cochin in October 97, Proc. Natl. Conf. Current trends in the ocean prediction with special Reference to Indian seas (Dec. 22-23, Kochi, India), pp. 90-94.

[16] La Fond E.C., 1961. The isotherm follower. *J. Mar. Res.,* **19** (In Press).

[17] Lynch J.F., Jin G., Pawlowicz R., Ray D., Plueddemann A.J., Chiu C.S., Miller J.H., Bourke R.H., Parsons A.R. and Muench R., 1996. Acoustic travel time perturbations due to shallow water internal waves and internal tides in the Barents Sea Polar Front: Theory and experiment. *The Journal of the Acoustical Society of America,* **99**(2), 803-821.

[18] Murty P.G.K., 2002. An Insight into Internal Waves in the Seas- around India. International Conference on Sonar - Sensors and Systems, *Proc. of ICONS, Kochi Naval Physical and Oceanographic Laboratory, India,* pp 525-532.

[19] Murthy P.G.K. and James V.V., 1996. Some aspects of Internal waves in the coastal waters off Cochin, *Proc. Second workshop Sci. Res. FORV Sagar Sampada,* pp 47-55.

[20] Murthy P.G.K. and Mohan Kumar N., 1996. Confirmatory checks for the internal waves in the coastal waters off Cochin, *Proc. Second workshop Sci. Res. FORV Sagar Sampada,* pp. 39-45.

[21] Murthy P.G.K. and Hareesh Kumar P.V., 1990. Response of coastal waters off Karwar to a deep depression. *Continental Shelf Research,* **11**(3), 239-250.

[22] Nishri A., Imberger J., Eckert W., Ostrovsky I. and Geifman Y., 2000. The physical regime and the respective biogeochemical processes in the lower water mass of Lake Kinneret. *Limnology and Oceanography,* **45**(4), 972-981.

[23] Rubenstein D., 1999. Observations of cnoidal internal waves and their effect on acoustic propagate ion in shallow water. *IEEE Journal of Oceanic Engineering,* **24**(3), 346-357.

[24] Sarma Y.V.B., Sarma M.S.S., Krishnamacharyulu, R.J. and Rao D.P., 1991. Subsurface oscillations at an oceanic station in the Bay of Bengal, *Ind.J. of Marine Sciences,* **20**, 204-207.

[25] Sridevi B., RamanaMurty T.V., Sadhuram Y. and Murty V.S.N., 2011. Impact of internal waves on the acoustic field at a coastal station off Paradeep, East coast of India. *Nat. Hazards.,* **57**, 563-576.

[26] Yang YJ, Tang TY, Chang MH, Liu AK, Hsu MK and Ramp SR., 2004. Soliton northeast of Tung-Sha island during the ASIAEX pilot studies. *IEEE Journal of Oceanic Engineering,* 29, 1182-1199.

The Journal of Acoustical Society of India : Vol. 46, No. 1, 2019 (pp. 10-18)

A Study of Attenuation of Underwater Acoustic Signal in Shallow Water Environment

R.P. Raju
Naval Physical and Oceanographic Laboratory, Kochi-682021
e-mail: rpraju@outlook.com

[Received: 01-10-19; Revised: 05-11-19; Accepted: 11-11-19]

ABSTRACT

High Frequency acoustic wave propagation is affected by suspended sediments in shallow water environment. The volume concentration of suspended particles of different sizes is known to follow a log-normal distribution with a tail of very fine particles. This distribution is used to model total attenuation as a function of frequency and particle size. The transmission loss in the presence of suspended particles is modelled and it shows a drastic increase, which in turn reduces the detection ranges of sonar. In the presence of 0.15% volume concentration of sediment particles of size 10 micron, the TL of a 70 kHz acoustic signal increases by more than 28 dB at a range of 100 m. The effect of distribution of particles on transmission loss is also studied in the paper. A case study on temporal variability of attenuation using a measured dataset, shows the importance of sediment particle distribution for accurate evaluation of the performance of a high frequency active SONAR.

1. INTRODUCTION

High frequency active SONARs play a major role in present day ASW scenario especially in shallow waters and estuarine coasts. The acoustic propagation of high frequency signals is hindered by high absorption in the medium and boundary scattering losses. In shallow water which is affected by terrigenic activities, suspended sediments is one of the factors responsible for attenuation of high frequency acoustic waves. Hence, it is important to study the effect of suspended sediment concentration on sound attenuation. The performance prediction for high frequency SONARs is usually done by using ray-theory based transmission loss modelling. In most of the cases the ranges achieved by such SONARs are by virtue of direct path only. In this paper, only the direct path propagation is considered for analysis of acoustic attenuation. Underwater acoustic attenuation studies have been done right from Second World War. In the absence of computational facilities, simple formula which included spreading loss and attenuation due to chemical processes was used for computation of Transmission Loss (TL) and detection ranges of SONARs. In this paper, the attenuation of acoustic signals due to suspended sediments is modelled using experimentally measured volume concentration values in literature.

2. UNDERWATER ACOUSTIC ATTENUATION MODEL

The propagation of underwater sound is affected by attenuation due to dissolved salts, viscosity and suspended particles. The physical mechanisms responsible for attenuation in sea water are chemical processes, viscous absorption and scattering.

The total attenuation of underwater sound in sea water is given by,

$$\alpha = \alpha_w + \alpha_v + \alpha_s \quad (1)$$

where, α_w is attenuation due to clear sea water,

α_v is attenaution due to viscous absorption

α_s is attenuation due to scattering by suspended particles

The attenuation due to clear sea water α_w, involves time lag between condensation and variation of acoustic pressure[1]. α_w is a function of frequency (*f*), temperature (T), salinity (S), acidity (pH), concentration of dissolved salts namely Magnesium Sulphate ($MgSO_4$) and Boric acid ($B(OH)_3$). The empirical formula for α_w is[2].

$$\alpha_w = \alpha_1 + \alpha_2 + \alpha_3 , \quad (2)$$

where, Fresh water contribution: $\alpha_1 = A_3 P_3 f^2$

$A_3 = 4.937 \times 10^{-4} - 2.59 \times 10^{-5} T + 9.11 \times 10^{-7} T^2 - 1.5 \times 10^{-8} T^3$, for $T \le 20°C$

$A_3 = 3.964 \times 10^{-4} - 1.146 \times 10^{-5} T + 1.45 \times 10^{-7} T^2 - 6.5 \times 10^{-10} T^3$, for $T > 20°C$

$P_3 = 1\text{-}3.83 \times 10^{-2} z + 4.9 \times 10^{-4} z^2$

$B(OH)_3$ contribution : $\alpha_2 = 0.101 \frac{f_1 f^2}{f_1^2 + f^2} e^{\frac{pH-2}{0.57}}$, $f_1 = 0.91 \left(\frac{S}{35}\right)^{0.3} e^{\frac{T}{35}}$

$MgSO_4$ contribution : $\alpha_3 = 0.56 \left(1 + \frac{T}{76}\right)\left(\frac{S}{35}\right)\left(\frac{f_1 f^2}{f_1^2 + f^2}\right) e^{\frac{z}{4.9}}$ $f_2 = 46.6\, e^{\frac{T}{18}}$

The attenuation due to viscous absorption depends on the frequency of the incident acoustic wave, volume concentration (ε) and density of suspended sediments which are basically scatterers. The expression for the viscous absorption is given by[2],

$$\alpha_v = (10 \log e^2)\left(\frac{\varepsilon k(\sigma-1)^2}{2}\left[\frac{s}{s^2 + (\sigma+\delta)^2}\right]\right) \text{dB m}^{-1} \quad (3)$$

where, $\delta = \frac{1}{2}\left[1 + \frac{9}{2\beta\langle a_s\rangle}\right]$ and $s = \frac{9}{4\beta\langle a_s\rangle}\left[1 + \frac{1}{\beta\langle a_s\rangle}\right]$

$\sigma = \frac{\rho_s}{\rho_o}$ where, ρ_s is the density of the scaterrer & ρ_o is the density of sea water

$\beta = \sqrt{\frac{\omega}{2\vartheta}}$ where, ω is the angular frequency and ϑ is kinematic viscosity of sea water

The attenuation due to scattering by suspended particles is modelled as scattering by a suspension of perfect fluid spheres[3] by Sheng and Hay. The expression is given by,

$$\alpha_s = (10 \log e^2)\left(\frac{\varepsilon K_\alpha x^4}{\langle a_s\rangle\left(1 + \varepsilon x^2 + \frac{4}{3}K_\alpha x^4\right)}\right) dB\ m^{-1} \quad (4)$$

where, $$K_\alpha = \frac{1}{6}\left(\gamma_k^2 + \frac{\gamma_\rho^2}{3}\right)$$

$x = k\langle a_s \rangle$ is dimensionless size parameter, $\langle a_s \rangle$ is mean particle radius,
k is wave number, ε is volume concentration of scatterers
γ_k and γ_p are compressibility and density contrasts[3]

Both $\propto_s$ and $\propto_v$ are functions of volume concentration of suspended particles. The volume concentration of suspended particles ε is a spatio-temporal parameter. Shallow water in naval harbours, ports, estuaries and river mouths will have very high concentration of suspended particles[4]. Deep water environment will have low volume concentration of suspended particles[4].

The effect of suspended particles on different attenuation terms in equation (1) is shown in figure 1. The following values have been considered for computation:

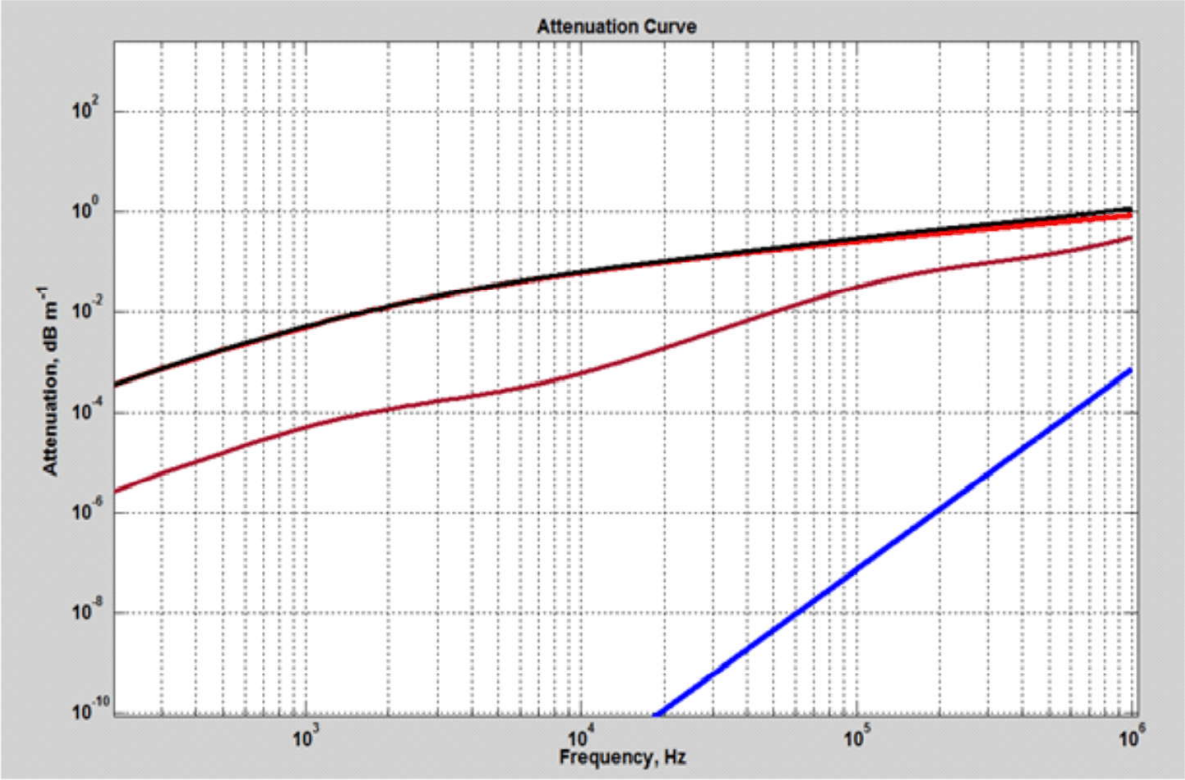

Fig. 1: Blue - α_s, Brown - α_w, Red - α_v and Black - α

$\langle a_s \rangle$ = 10 μm, ε = 0.0015 (Volume concentration of quartz particles corresponding to 4 kg m^{-3}), γ_k = 0.93, γ_ρ = 0.77, ϑ = 8.532 × 10^{-7} at 27°C, ε = 1, σ=2.65, depth = 15 m, T=27°C and S = 35 psu.

The attenuation due to viscous absorption, α_v is maximum among the three attenuation terms. The effect of α_s is minimalthroughoutthe frequency range considered.The total attenuation as a function of different particle sizes with same volume concentration e of 0.0015 is plotted in figure 2. It is observed that beyond 1 kHz, the attenuation increases with increase of particle sizeand below 1 kHz, higher particle size (10 x 10^{-5} m) give lesser attenuation.

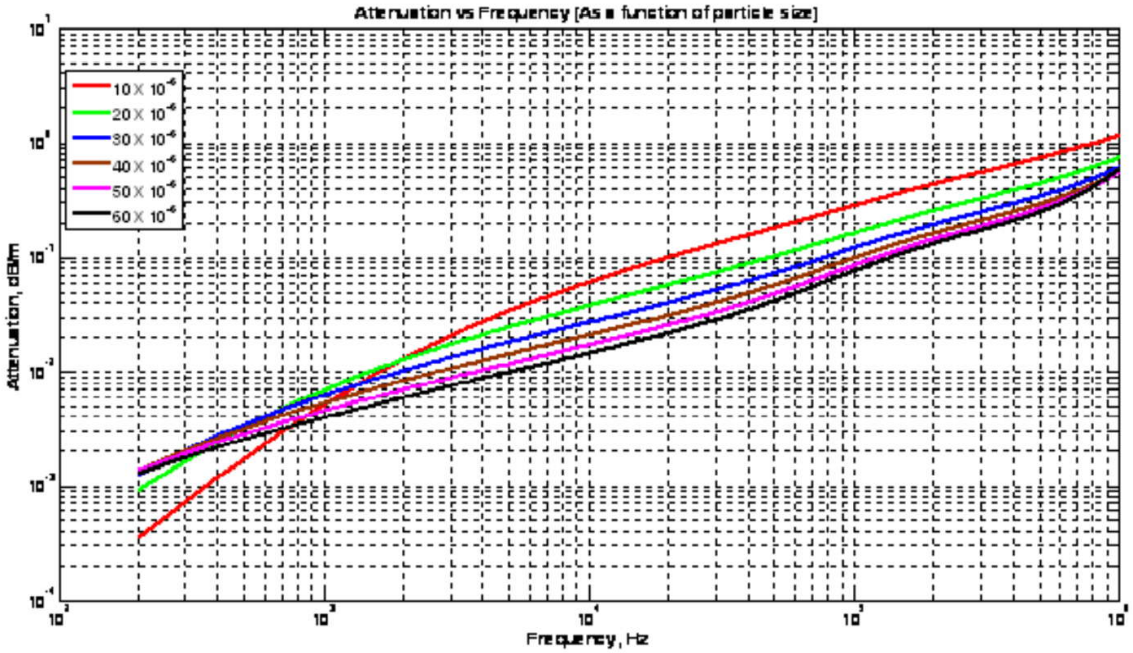

Fig. 2: Attenuation vs. Frequency (Different Particle Sizes)

The effect of different particle sizes (volume concentration ε of 0.0015) on attenuation of acoustic wave of different frequency is plotted in figure 3. It is observed that the total attenuation, for a fixed volume concentration of ε of 0.0015, increases with particle size up to 10 micro-meter and there after the total attenuation decreases when particle size increases.

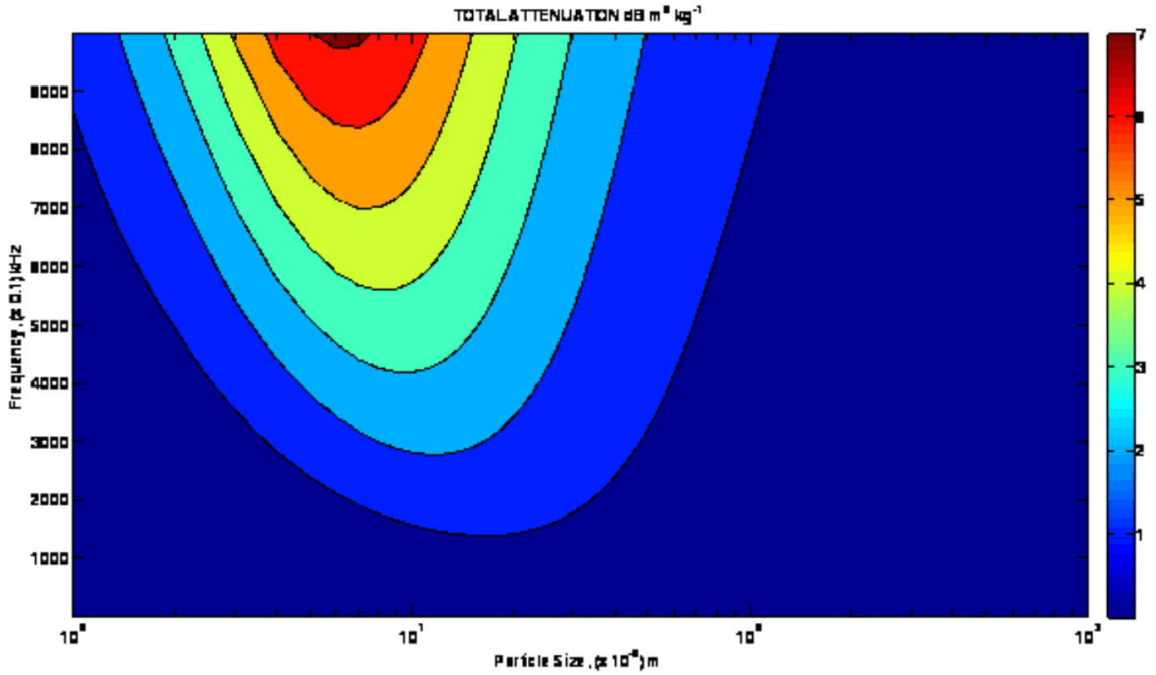

Fig. 3: Total Attenuation (Frequency vs. Particle Size)

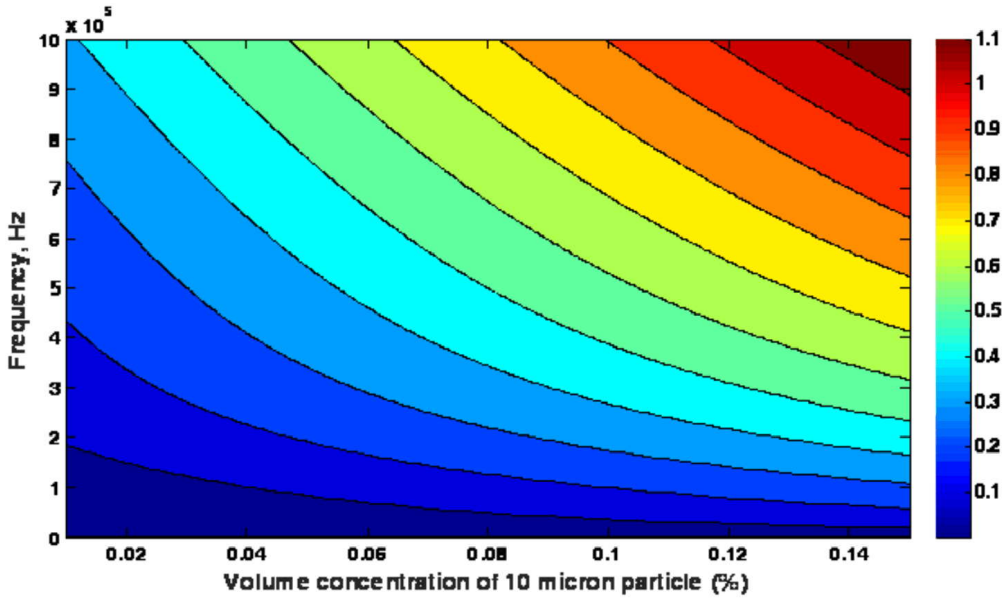

Fig. 4: Total attenuation (Frequency vs. Volume concentration)

The effect of different volume concentrations of 10 μm (micron) is plotted in figure 4.It is observed that the total attenuation for a 10 μm particle size increases with the concentration of the particle and the frequency of propagation.The TL vs. range plot for 70 kHz during the presence and absence of suspended particles (volume concentration ε of 0.0015) for a direct path source-receiver configuration is shown in figure 5.It is seen that the TL increases significantlywith range in the presence of the suspended particle in the water column whereas the TL is found to be almost constant with range after 200m. The TL is computed as a combination of spherical spreading loss and medium attenuation loss.

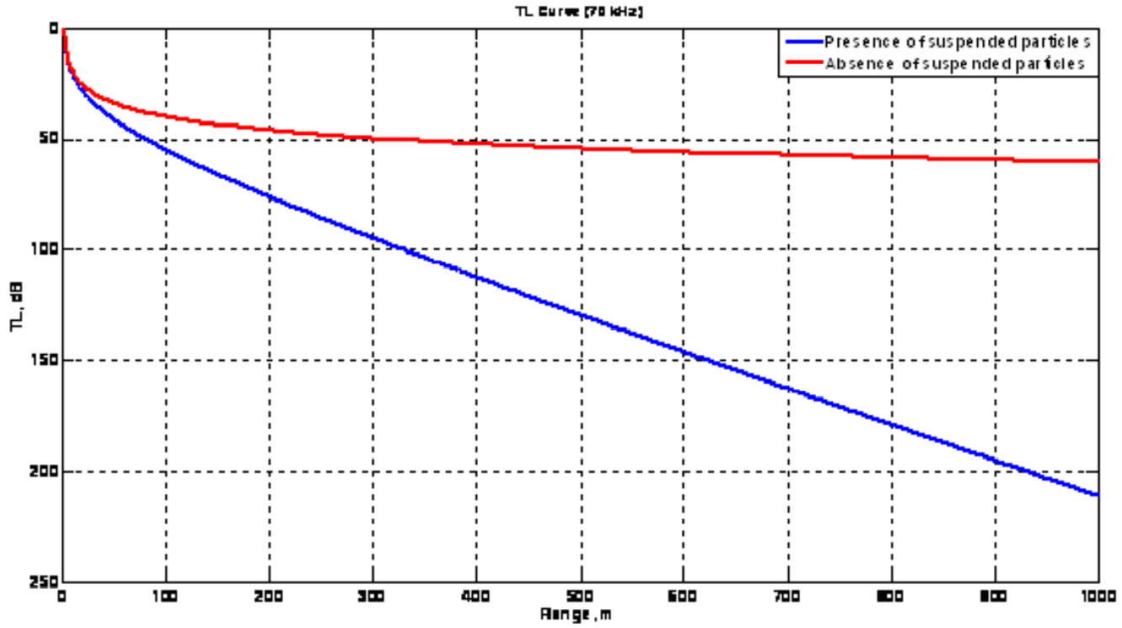

Fig. 5: Plot of Transmission Loss(TL) vs. Range

The effect of variation in volume concentration of particle size10 micron on TL with respect to range for 70 kHz and 700 kHz is plotted (Figure 6 and 7). It is seen that for 70 kHz frequency, the TL increases with range slower than for 700kHz. However, the loss is high at 700 kHz.

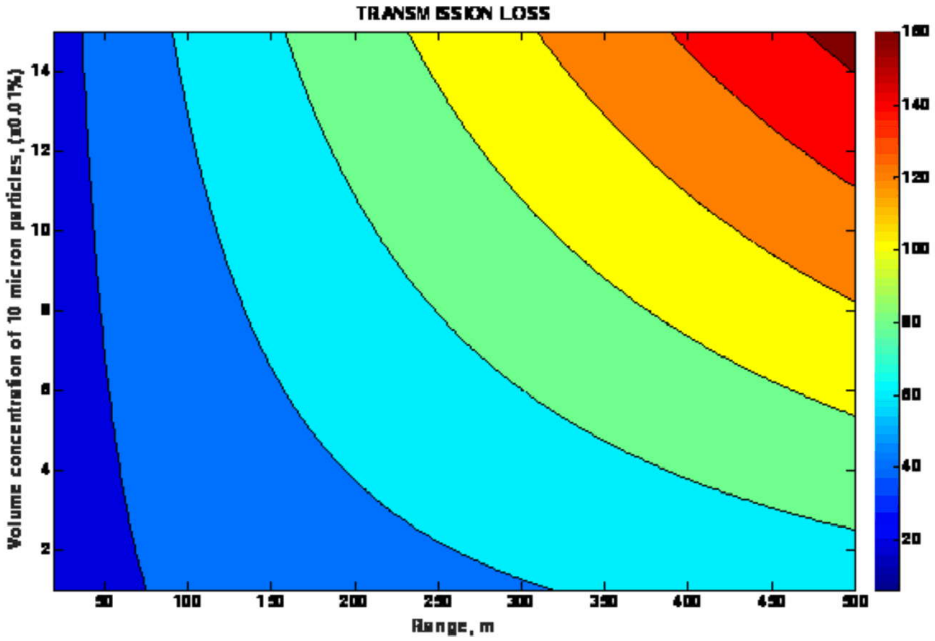

Fig. 6: Transmission Loss (Volume Con centration vs. Range) for 70 kHz

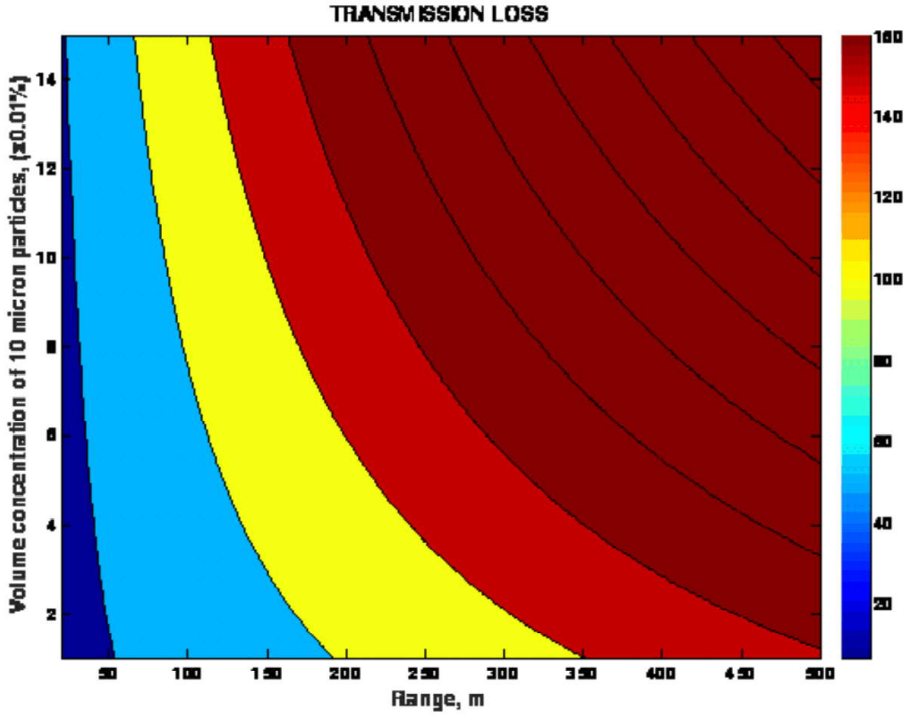

Fig. 7: Transmission Loss (Volume Concentration vs. Range) for 700 kHz

3. QUALITATIVE STUDY USING DATA

In literature it is seen that volume concentration of different suspended particle radii follows a log-normal distribution[5] with peak value around 10 μm. A tail of fine particles is also seen in the suspended particle radius distribution. This distribution curve is found to be consistent for different near coastal regions and turbid waters. Hence this curve is used to read the sediment concentration against the particle sizes. The temporal variation of sediment grain-size distribution data collected 1 km off Dutch coast in 11 m water[5] is used to compute attenuation. This study was undertaken to understand the response to varying forcing of suspended particulate matter and chlorophyll-a (CHL-a) in a coastal turbidity maximum zone. The observed peak volume concentration with respect to suspended particle size during May 2011, October 2011 and February 2012 has been reported at 9 μm, 6.5 μm and 10.5 μm respectively. It is assumed that the particles in the measured distribution[5] are quartz particles.

4 RESULTS AND DISCUSSION

The temporal variation in total attenuation for the three days of observation for different seasons arecomputed (Figures 8, 9, 10) using the measured data. Figure 8 shows two peaks in the attenuation for the sediment size versus frequency plot during the observation on 11 May 2011, while the other observations show only a single peak in the attenuation.

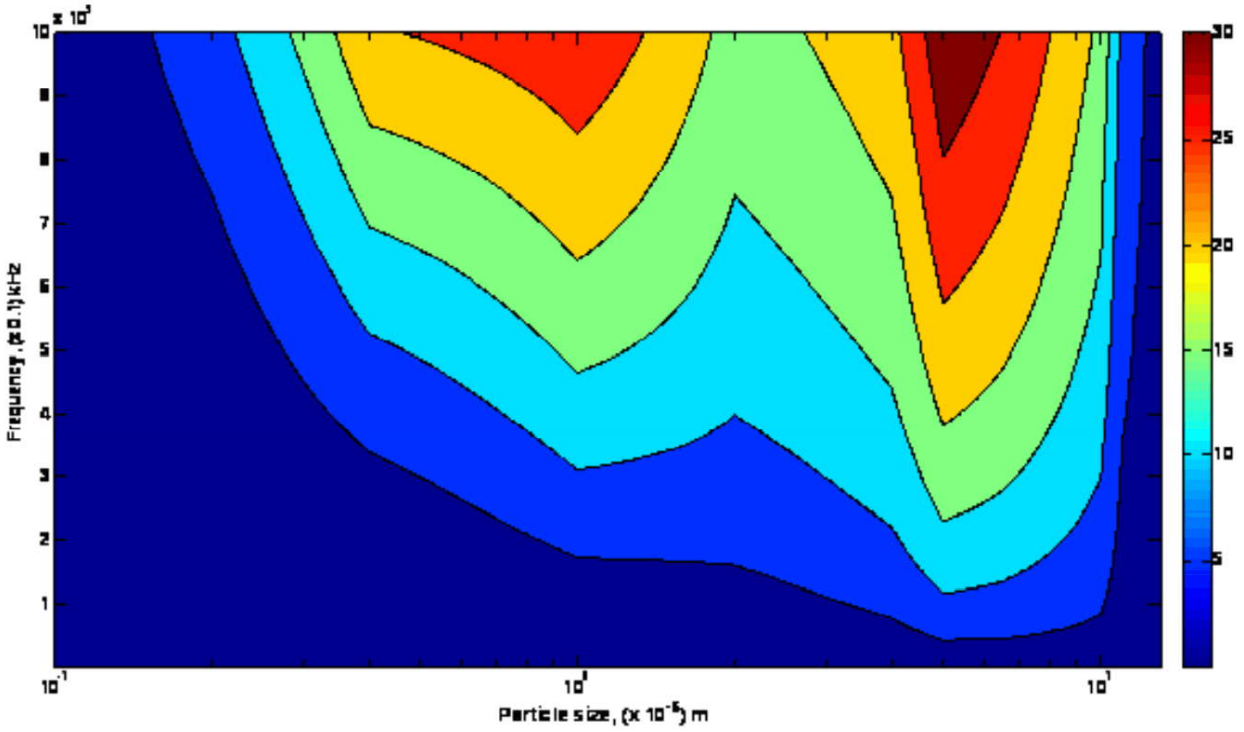

Fig. 8: Total attenuation (dB m^{-1}) during May 2011

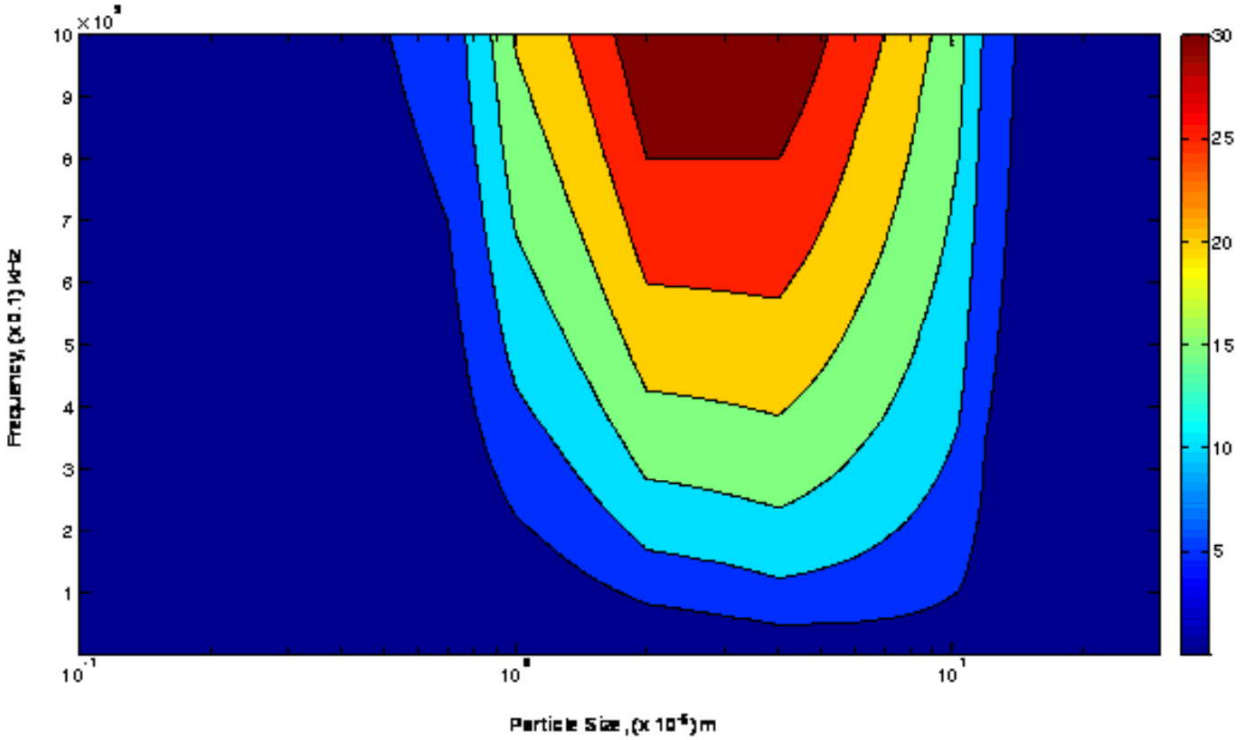

Fig. 9: Total attenuation (dB m^{-1}) during October 2011

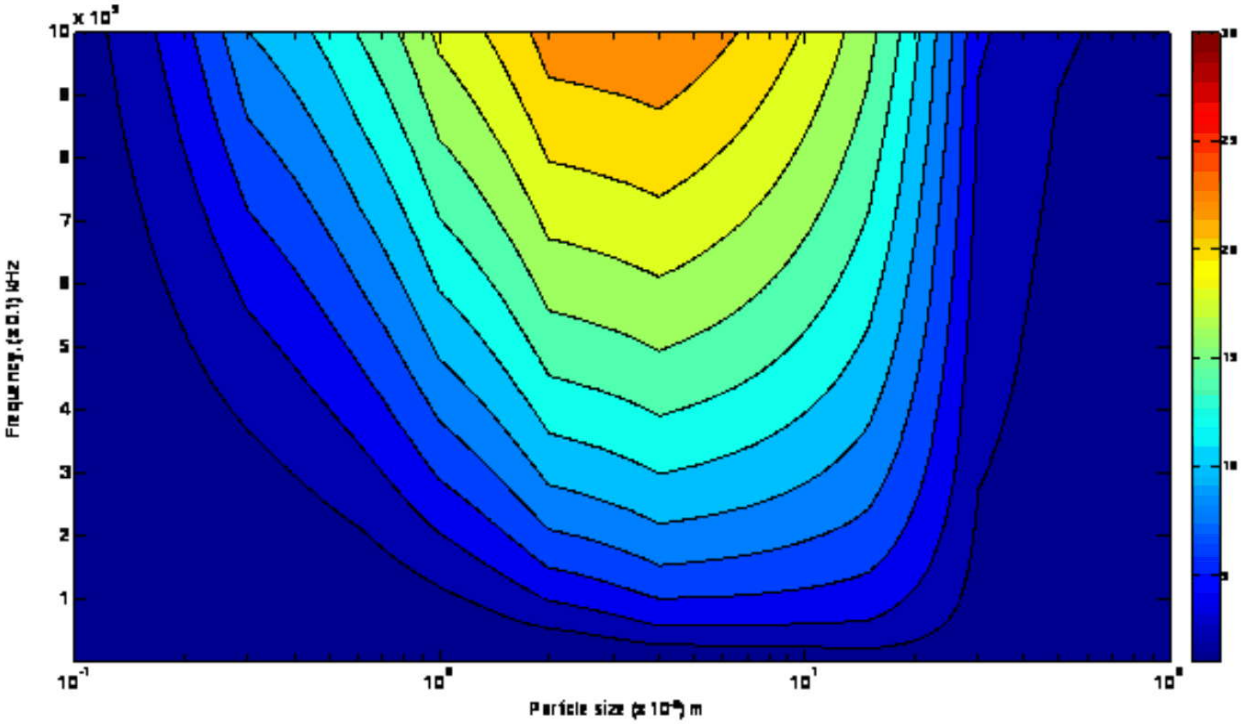

Fig. 10: Total attenuation (dB m^{-1}) during February 2012

The initial analysis of the attenuation model results (Figures 1, 2) in the presence and absence of suspended particles shows a marked bias. At 2 kHz, total attenuation is 0.001 in the presence of suspended particles which is hundred times more than the attenuation due to chemical processes.

At higher frequencies (600-1000 kHz), a peak is observed in total attenuation for particle size around 10 microns (Figure 3). These frequency ranges are used by acoustic imaging SONARs. The higher TL in case of such SONARs in turbid shallow waters (with high particle concentration of 10 μm) is observed in figure 7, as well. In figure 6, TL plot for 70 kHz is considered, that is the usual frequency for harbour protection SONARs. The variation in TL mosaics in the presence and absence of suspended particles is clearly seen. The TL increases rapidly with frequency as the volume concentration of suspended particles increases from 0.01% to 0.15%.The twin peaks in attenuation in figure 8 corresponds to peaks in the measured volume concentration distribution6.These twin peaks disappear and centre around 3-4 μm during October 2011 and February 20126 (Figures 9, 10). The effect of suspended particles in shallow water on propagation of high frequency acoustic waves is pronounced as its concentration increases. The performance of High Frequency underwater acoustic systems are very much affected by the concentration of different sizes of suspended sediment particles present in the water column. Hence, the attenuation due to suspended particle concentration to be included in TL calculations for accurate performance evaluation of high frequency sonar systems.

5 ACKNOWLEDGEMENT

The author would like to thank Shri S VijayanPillai, Director, for his encouragement to take up research on high frequency ocean acoustics.The author would like to express his gratitude to Dr KG Radhakrishnan, Group Director (Ocean Sciences) for the suggestions that greatly improved the manuscript. The authors would also like to acknowledge the encouragement provided by Dr PV Hareesh Kumar, Director (Science and Technology), and Dr KV Sanilkumar, Associate Director (Ocean Sciences).

6. REFERENCES

[1] Van Moll C.M., Ainslie M.A. and Vossen R., 2009. "A simple and accurate formula for absorption of sound in seawater" *IEEE journal of ocean engineering,* **34**(4), 610-616.

[2] Sheng, Jinyu and Alex E. Hay, 1988. "An examination of the spherical scatterer approximation in aqueous suspensions of sand." *The Journal of the Acoustical Society of America,* **83**(2), 598-610.

[3] Hay Alex E., 1983. "On the remote acoustic detection of suspended sediment at long wavelengths." *Journal of Geophysical Research, Oceans,* **88**(12), 7525-7542.

[4] Urick R.J., 1983. Principles of Underwater Sound. *McGraw Hill Book Company.*

[5] Richards S.D., Heathershaw A.D. and Thorne P.D., 1996. "The effect of suspended particulate matter on sound attenuation in seawater." *The Journal of the Acoustical Society of America,* **100**(3), 1447-1450.

[6] Van der Hout C.M., Witbaard R., Bergman M.J.N., Duineveld G.C.A, Rozemaizer M.J.C. and Gerkema, T., 2017. "The dynamics of suspended particulate matter (SPM) and chlorophyll-a from intratidal to annual time scales in a coastal turbidity maximum." *Journal of sea research,* **127**, 105-118.

The Journal of Acoustical Society of India : Vol. 46, No. 1, 2019 (pp. 19-27)

Effect of Multipath Arrival Structure on Temporal Coherence of High Frequency Broadband Transmissions in Shallow Water

Sreeram Radhakrishnan, Anil Kumar K and Elizabeth Shani
Naval Physical and Oceanographic Laboratory, Thrikkakara, Kochi, India
e-mail: sreeramr@gmail.com

[Received: 01-10-19; Revised: 11-10-19; Accepted: 11-11-19]

ABSTRACT

Results of high frequency impulse response measurements made in a shallow water channel are presented to analyze the temporal coherence of broadband acoustic signals. The acoustic propagation experiment was conducted at a shallow water location in the South Eastern Arabian Sea off the west coast of India in a water depth of 72 m. High frequency broadband signals (20-25 kHz) were transmitted from a depth of 15 m and received at two ranges, 610 m and 1700 m by three hydrophones located at 8 m, 18 m and 58 m depths. Concurrent measurements of sound speed profiles and sea surface wave height were also made. Impulse response measurements are utilized to estimate the temporal coherence of acoustic signals and then correlated with the multipath arrival structure which is a characteristic feature of acoustic propagation in shallow water. At 610 m range, the 8m depth receiver shows high temporal coherence with a coherence time of about 6 s and seems to be the optimal receiver depth for optimal underwater acoustic communication. At 1700 m range, the 18 m depth receiver appears to be the best receiver depth. The multipath arrival structure at this depth features a single dominant transmission path which is an ideal situation for establishing underwater communication.

1. INTRODUCTION

Acoustic channel characterization helps to determine, for a given range of frequencies, the limitations imposed by the oceanic environment on the exploitation of coherent signal structure [1-3]. This understanding is required in order to optimize sonar signal processing structures (*e.g.* channel conditioning, especially in shallow water), for wideband signal and processor design and for acoustic propagation modeling. Time spreading measurements of high frequency acoustic signals provide an indirect measure of the channel bandwidth [4-6]. Frequency bandwidth of the propagating medium is critical to the design of sonar and underwater communication systems. Increasing the bandwidth enhances sonar performance, but the channel impulse response (CIR) determines the upper limit one may achieve. Hence, the information present in the CIR is required to optimize the transmit pulse of the sonar. The time spreading characteristics obtained from CIR measurements determine the pulse length, type of the pulse and the frequency bandwidth.

Acoustic signals propagating through the ocean fluctuate with time and the rate of signal fluctuation can be described by the temporal coherence of the signal. Many studies on low frequency sound fluctuations have been carried out in deep oceans over long ranges [7-9]. The results from these measurements were presented in terms of the signal phase rate, which is the inverse of signal coherence time. A few measurements on temporal coherence of acoustic signals have been carried out in shallow water to analyze the effect of oceanographic variability such as internal waves. Badiey *et al*. [10] studied temporal coherence of broadband acoustic signals in very shallow coastal regions. Rouseff *et al*. [11] measured and modelled temporal coherence of acoustic modes in the presence of internal waves. Yang [12] described shallow water measurements of temporal coherence of acoustic signals using data from three different experiments and analyzed data to address the deviation from deep water measurements. Siderius *et al*. [13] studied the effects of ocean thermocline variability on non-coherent underwater acoustic communications and demonstrated that the frequency-shift-key modulation performance is strongly affected by diurnal cycles in the thermocline.

In this paper, the results of temporal coherence of high frequency broadband signals transmitted in a shallow water multipath environment are presented. Linear Frequency Modulated (LFM) signals were transmitted in 20-25 kHz frequency band from a source at 15 m depth and received at hydrophones located at 8, 18, 58 m depths in a water depth of 72 m. The transmissions were made for two source-receiver ranges, 610 m and 1700 m. In order to analyze the effect of propagating medium on individual paths, the time dispersed CIR was estimated by matched filtering the received time series with the transmitted waveform. Estimation of CIR allows for resolution of multipath arrivals in a shallow water environment. The individual arrivals can then be analyzed for characterizing the effect of the propagating medium. A ray theory based propagation model is used to identify eigenrays and ascertain their travel times for various source receiver configurations realized during the experiment. In addition, it is used as an interpretive tool to analyze and differentiate between arrival structures at different depths in the presence of a depth-dependent sound speed profile.

In particular, the purpose of this study is to analyze the effect of rough sea surface and thermocline on the temporal coherence of acoustic signals. Temporal coherence is obtained from the measurements of CIR. The CIR of the first ping is taken as reference and is cross correlated with the CIR of the subsequent pings. In addition, CIR is also used to identify individual multipath arrivals and analyze their amplitude fluctuations. Once the dominating arrival is identified, the principal cause of loss of temporal coherence can be attributed to the fluctuation of that arrival. For instance, if direct path is the dominant arrival, any mechanism affecting the water column sound speed profile will be the principal cause of loss of coherence. Sea surface roughness will be responsible for loss of coherence of acoustic signals if the surface path turns out to be the dominant arrival.

Analysis is carried out on data recorded by three hydrophones at the depths of 8, 18 and 58 m. The 8 m hydrophone is placed close to the sea surface and is expected to receive a strong surface bounce path at low grazing angles in addition to the direct path. The temperature profile measured during the experiment indicates that the thermocline is confined to a depth range of 25-55 m. Hence, it will not have any considerable effect on acoustic signals arriving at the 8 m hydrophone, which is sufficiently above the thermocline. However, the effect of sea surface roughness will be evident at this depth and cause the temporal coherence to drop as roughness increases. The second hydrophone located at a depth of 18 m is positioned just above the thermocline layer but away from the sea surface boundary. The third hydrophone is located at 58 m depth just below the thermocline layer. The acoustic signals received by this hydrophone will be analyzed for observations of loss of coherence due to thermocline variability in the water column. The coherence of direct path arrivals as a function of time will be affected by thermocline oscillations. The sea surface bounce path arriving at this depth will have a steep angle of propagation and be highly attenuated.

The paper is organized as follows. Section 2 gives a comprehensive definition of temporal coherence as applicable to detection and localization studies. The acoustic propagation experiment and the concurrent

environmental measurements are described in Section 3. Data analysis and interpretation in terms of channel impulse response and temporal coherence are provided in Section 4. Summary and concluding remarks are given in Section 5.

2. TEMPORAL COHERENCE OF ACOUSTIC SIGNALS

The knowledge of signal coherence-time is useful for many applications, such as narrow band detection, matched-field processing and adaptive signal processing. Temporal coherence of the signal is given by the autocorrelation of the acoustic signal normalized by the average signal energy [12].

$$\rho(\tau) = \frac{(p\times(t)p(t+\tau))}{(p\times(t)p(t))(p\times(t+\tau)p(t+\tau))} \tag{1}$$

The following equation may be used to measure the signal temporal coherence of broadband signals separated by a delay time τ,

$$\rho(\tau) = \frac{[p\times(t)\otimes p(t+\tau)]max}{[p\times(t)\otimes p(t)]max[p\times(t+\tau)\otimes p(t+\tau)]max} \tag{2}$$

where $[p \times (t) \otimes p(t + \tau)]$max means the maximum value of the cross-correlation of the two time series or the convolution of the time-reversed signal with the other signal and < > denotes the ensemble average wherein the coherence is estimated by averaging over 5 datasets. * denotes the complex conjugate. As shown in Eq. (2), the temporal coherence of a signal is a function of signal transmission time *t*. The higher the signal fluctuation, the faster the temporal coherence decreases with time. The measurement near time t represents the instantaneous signal coherence-time. The signal coherence-time is defined as the time by which signal becomes uncorrelated, that is, when the temporal coherence reduces to 1/e (= 0.37). In narrowband detection and localization, the signal coherence-time determines the maximum time of integration in order to estimate temporal processing gain. It determines for how long a signal remains coherent or degrades with time. It could have a large variance depending on the signal frequency and the time scale of the oceanographic processes affecting the signal.

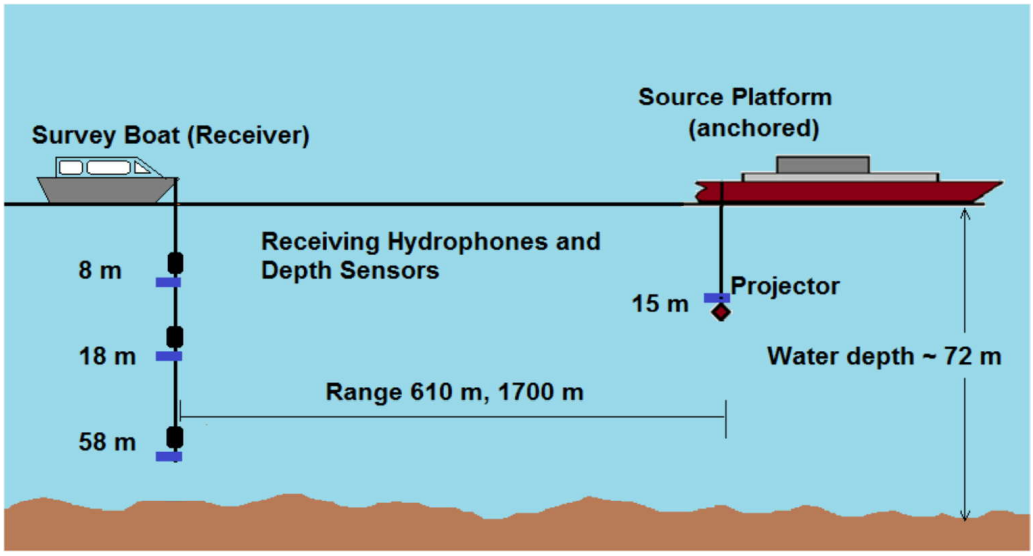

Fig. 1: Schematic of the shallow water acoustic channel characterization experiment conducted on 4 Nov 2015 at a shallow water location in the Arabian Sea in water depth of 72 m.

3. ACOUSTIC PROPAGATION EXPERIMENT

An acoustic propagation experiment was conducted and impulse response measurements were made on Nov 4 2015 at a shallow water location in the Arabian Sea off the west coast of India. Figure 1 shows the schematic of the source receiver geometry realized during the experiment. A hydrographic survey vessel was anchored in a water depth of 72 m which served as the source platform. Concurrent measurements of temperature and salinity profiles and sea surface wave height and direction were also carried over the course of the acoustic experiment at the shallow water location.

3.1 Environmental measurements

Conductivity-Temperature-Depth (CTD) casts were made to measure temperature (T) and salinity (S) profiles. Sound velocity profiles were computed from T and S profiles and are observed to follow the temperature profile which featured a weak thermocline in the depth range of 30-55 m. The left panel of Fig. 7 shows the sound speed profiles estimated using CTD measurements made at different times during the acoustic experiment. The profiles collected from 1112 hrs to 1150 hrs showed minimal temporal variation during the course of the experiment. The water column sound speed showed a top to bottom variation of ~1.5 m/s.

Directional wave height spectra were measured during the experiment using a bottom mounted Workhorse Sentinel Acoustic Doppler Current Profiler[14]. The right panel shows the wave height spectra measured during the experiment at half hourly intervals. During the experiment, wind speed was 3.6 m/s, significant wave height was 1.4 m and RMS wave height was 1 m, corresponding to sea state 3. It was observed that the surface waves predominantly came from north with a peak period of ~13 s.

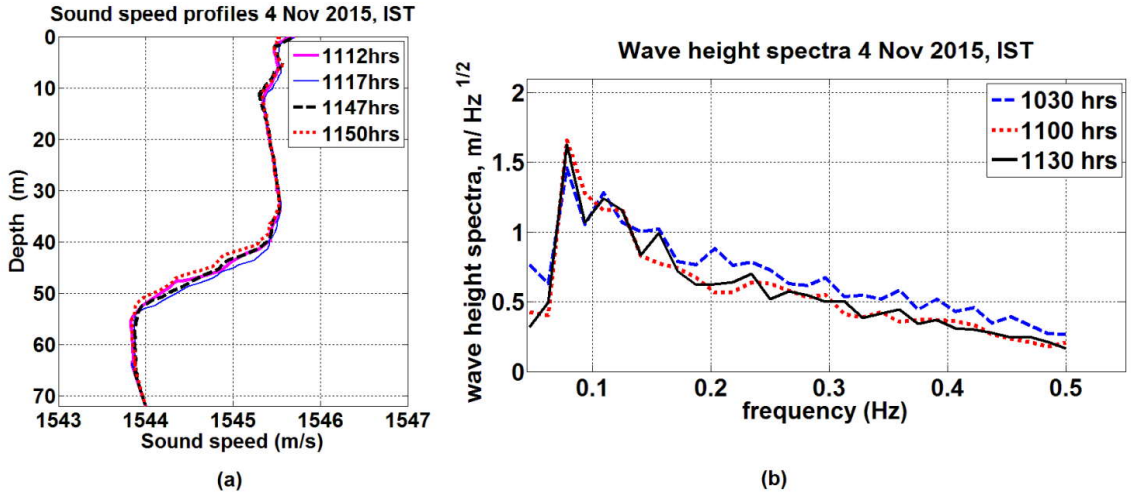

Fig. 2: LEFT: Sound speed profiles estimated from CTD measurements made during the experiment. The 610 m range transmissions were made from 1112-1117 hrs and the 1700 m range transmissions were made from1147-1150 hrs on 4 Nov 2015. RIGHT: Wave height spectra measured during the acoustic experiment showing a swell peak at 0.078 Hz (peak period of ~13 s). Data represents 30 min average.

3.2 Acoustic measurements

An omni-directional broadband projector was suspended from an anchored ship at a depth of 15 m and used for transmitting linear frequency modulated (LFM) pulses of length 50 ms in frequency band of 20-25 kHz. Transmissions were received on three hydrophones deployed from a boat at 8, 18 and 58 m depths in a water depth of 72 m. The hydrophone and projector depths were monitored by depth sensors. The peak transmitting voltage response (TVR) of the projector is 150 dB re 1μPa/ V at 1m at 21 kHz. It is

found to vary from 149 dB re 1μPa/V at 1m at 20 kHz to 148 dB at 25 kHz. Signals were generated and amplified using an Instrument Inc. L2 power amplifier. A monitoring hydrophone was placed near the projector to monitor its source level throughout the course of the experiment. A survey boat was used as the receiving platform and the signals were received by B & K 8105 hydrophones deployed from the boat. Received signals were sampled at 51.2 k samples/s.

Analysis is presented for measurements carried out at two ranges of 610 m and 1700 m based on the data recorded by the three hydrophones. The 8 m hydrophone being close to the sea surface is expected to receive a strong surface bounce path at low grazing angle which may show significant fluctuations due to receiver platform oscillations. The second hydrophone located at a depth of 18 m is positioned well above the thermocline layer as well as away from the sea surface boundary. The third hydrophone is located at 58 m depth located just below the thermocline layer. The received time series is used to estimate impulse response and effective bandwidth. As the source ship was anchored, the projector depth variation was minimal during the experiment.

Table 1. Transmitted waveform, bandwidth, pulse length and geometry of the data used for analysis. Source depth is 15 m

S No	Frequency Band (kHz)	Pulse Length (ms)	Bandwidth (kHz)	Time Bandwidth product (TW)	Receiver Depths (m)	Source Receiver Ranges (m)
1	20-25	50	5	250	8, 18, 58	610, 1700

The broadband signals that were transmitted to study the effect of propagating medium for different source receiver configurations are listed in Table 1. The dataset spans 6 source receiver configurations. Note that the TW product is high for each of the transmissions suggesting that they are Doppler tolerant. In many previous studies, the LFM signals are found to be suitable to study the effects of time dispersion in a shallow water multipath environment [4, 15, 16]. Each set of transmission consists of 20 pings with a pulse repetition interval of 300 ms and lasts for a duration of ~6 s. The LFM pulses used as probe signals are of width 50 ms to ensure that they are longer than the expected multipath spread of the underwater channel.

The sea surface acoustic roughness can be quantified in terms of the Rayleigh parameter given by $\chi = 2$ kHsin θ_g where k = acoustic wavenumber, H = RMS wave height and θ_g= grazing angle. For an RMS wave height of ~1.15 m observed during the experiment and the central frequency of 22.5 kHz, the value of Rayleigh parameter (χ) was found to vary from 5.1 to 15.7 for grazing angles ranging from 1.8 - 5.7. The values of χ much greater than 1 suggest that the sea surface is acoustically rough and will contribute to considerable amount of scattering. The effect of scattering is evident in measured acoustic data, especially at 610 m range measurements where the surface grazing angles are steep.

4. DATA ANALYSIS AND DISCUSSION

The impulse responses in the form of matched filter envelopes measured at the two ranges at three different depths are compared in Fig. 3. The first six multipath arrivals can be clearly identified from the matched filter envelope responses for each of the depths. They are direct (D), surface (S), bottom (B), surface-bottom (SB), bottom-surface (BS) and surface-bottom-surface paths (SBS). To measure the relative strength, the matched filter envelopes for the 3 depths at each range are normalized with respect to the strongest arrival. At 610 m range, the strongest arrival observed is the direct path at 58 m depth. Its magnitude is set to 1 and all other arrivals are normalized relative to it. At 610 m range, the direct and surface paths overlap with each other at 8 m and 18 m depths. The multipath spread varies between 15-18 ms for the first six arrivals at these depths. At 58 m depth, direct and surface-bounce paths are well separated and the time spread is close to 24 ms which is well within the sounding signal length of 50 ms. At this range, the effect of refraction on the propagating signals is minimal.

At 1700 m range, the strongest arrival is received at the 18 m depth hydrophone. The overall multipath spread varies between 12-20 ms. The effect of refraction becomes important at this range. As the 8 m depth receiver is close to the sea surface, the direct path is highly attenuated. In contrast, the direct path arrivals at 18 m and 58 m depths are fairly strong. Further, the amplitude of surface-bounce path is expected to fluctuate significantly being close to the sea surface.

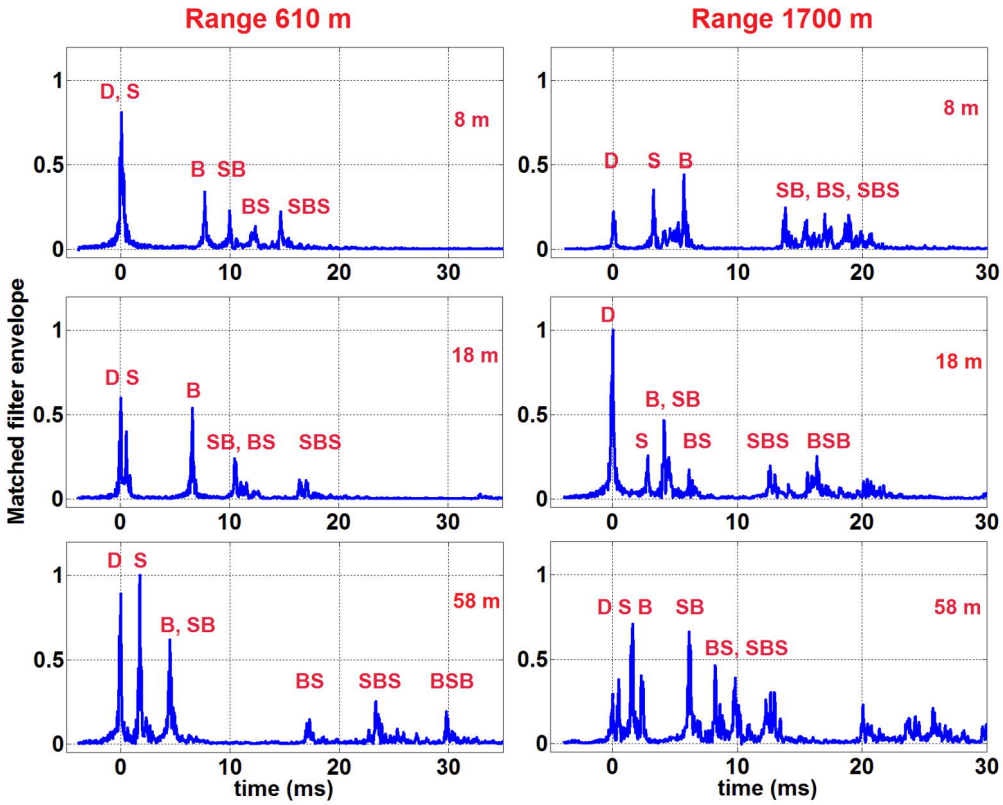

Fig. 3: Each panel shows a single LFM chirp impulse response in the form of normalized matched filter output envelope as a function of delay time corresponding to three receiver depths 8 m, 18 m and 58 m (as indicated). Each of the multipath arrivals are identified. Source depth is 15 m. Source receiver ranges are 610 m (left) and 1700 m (right). Time of arrival of direct path is aligned to zero.

Temporal coherence of acoustic signals propagating through a shallow water channel is highly influenced by non-stationary boundaries such as the water surface. When the acoustic roughness of the sea surface is high, it will result in sea surface scattering reducing the amplitude of specular reflected arrival. The bottom boundary being stationary, does not contribute to the loss of signal coherence as a function of time. Higher ping to ping variability will lead to lowering of coherence time drastically which in turn affects performance of sonar and underwater communication systems. Acoustic signals are also adversely affected by ocean volume inhomogeneities such as changes in the water column sound speed profile. The latter is caused mainly by internal waves and turbulence.

In this analysis, we present and compare the temporal coherence of LFM signals at three depths and two source-receiver ranges in the 20-25 kHz frequency band. Each set of transmission consists of 20 pings with a pulse repetition interval of 300 ms and lasts for a length of ~6 s. In the present analysis, 5 such sets of transmissions are processed and the temporal coherence of broadband signal is estimated as the ensemble average of the 5 sets. The average temporal coherence is then plotted as a function of delay

time. The results of temporal coherence are obtained using Eq. (2) and compared for the hydrophone depths of 8, 18 and 58 m. The results are presented in Fig. 4 for the two ranges separately. The plot of temporal coherence as a function of delay time gives an estimate of average signal coherence time. The temporal coherence can be analyzed with respect to coherence time of the signal. Conventionally, it is defined by the time delay at which the coherence value drops to 1/e (~0.37) of the reference value which here is taken as 1. This level is marked in each of the plots.

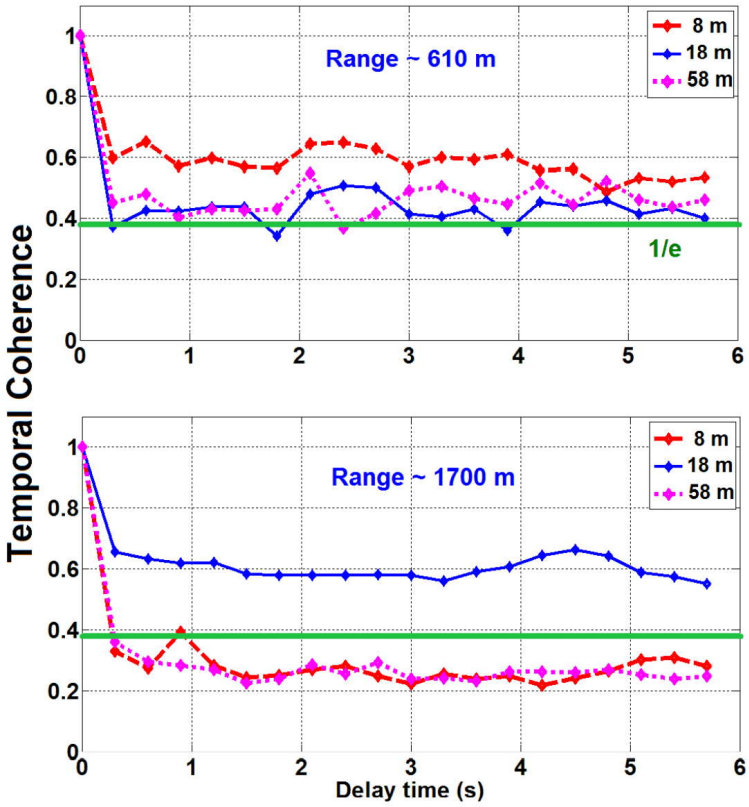

Fig. 4: Average Temporal Coherence of 20-25 kHz, 50 ms LFM pulses over a delay time of 6 seconds. Source depth is 15 m and range is 1700 m. Signals received at 3 depths, 8 m, 18 m and 28 m are compared to examine the dependence of coherence on depth.

At 610 m range, the coherence time is greater for the 8 m receiver depth as compared to 18 m and 58 m depths. This can be attributed to two reasons. One is that the surface reflected path is stronger at 8 m depth relative to 18 m and 58 m depths where the grazing angles are steeper contributing to higher surface reflection loss. The other is the presence of a relatively uniform sound speed profile in the top 30 m. The temporal coherence plot at 1700 m range shows that the 18 m depth receiver is an optimal receiver position with a very high coherence time (> 6 s). The CIR data corresponding to 18 m depth shows a near ideal impulse response function featuring a single dominant transmission path. Also, the multipath time spread is less than 10 ms for the first 4 arrivals. The presence of a single dominant path results in considerable increase in the coherence time of the signals received by the 18 m depth receiver making this configuration superior to the other two depths (8 m and 58 m) for effective transmission of acoustic data. Higher coherence time can be achieved by optimizing the relative depth of the receiver with respect to the source depth in a shallow water environment. It turns out that at a range of 610 m, the 8 m depth receiver has a higher coherence time (> 6s) but as the range is increased to 1700 m, the 18 m depth receiver retains its coherence longer than the 8 m depth receiver.

5. SUMMARY AND CONCLUSION

A shallow water acoustic experiment was conducted and channel impulse response measurements were made at the shallow water benchmark site in the Arabian Sea. Channel impulse response measurements were made to determine multipath arrival structure and thereby understand the shallow water propagation characteristics. In addition, channel impulse response measurements were utilized to estimate temporal coherence of acoustic signals. The experimental data set collected and the analysis carried out will serve as reference for testing and benchmarking underwater communication system prototypes. Data collected at two source receiver ranges, 610 m and 1700 m are presented. Analysis is carried out on signals transmitted from a depth of 15 m and recorded by three hydrophones at the depths of 8, 18 and 58 m in a water depth of 72 m.

At 610 m range, the 8 m depth receiver was observed to be the best receiver depth with high temporal coherence. At this depth, the CIR data shows a single dominant transmission path. At 1700 m range, the time spread in channel impulse response reduces considerably as does the amplitude of received signals. The CIR data at 1700 m range shows a time spread of less than 10 ms for the first four arrivals which includes direct, surface, bottom and surface-bottom path arrivals. The corresponding time spread at 610 m range is ~20 ms. At 1700 m range, the 18 m depth receiver was the highest coherence time. At a range of 610 m, the 8 m depth receiver has a coherence time exceeding 6 s but as the range is increased to 1700 m, the 18 m depth receiver was observed to have a higher coherence time than that of the 8 m depth receiver. Hence, the configurations with a single dominant arrival were found to have the highest coherence time.

6. ACKNOWLEDGEMENTS

The authors express their sincere gratitude to Shri. S Vijayan Pillai, Director, NPOL for providing ample facilities and encouragement to complete the work. Authors also appreciate the assistance extended by the ship officers and crew and the fellow scientists that helped in collecting high quality data.

7. REFERENCES

[1] Catipovic L., 1990. "Performance limitations in underwater acoustic telemetry," *IEEE J. Ocean. Eng.* **15**, 205-216.

[2] Kilfoyle D.B. and Baggeroer A.B., 2000. "The state of the art in underwater acoustic telemetry", *IEEE J. Ocean. Eng.,* **25**, 4-27.

[3] Preisig J.C., 2005. "Performance analysis of adaptive equalization for coherent acoustic communications in the time-varying ocean environment," *J. Acoust. Soc. Am.* **118**, 263-278.

[4] Hines P.C., Collier A.J. and Hutton J.S., 1996. "Time spreading at high frequency in a shallow water channel," *DREA Technical Memorandum,* **96**, 209.

[5] Adams S.L. and Doubek J.W., 1977. "Frequency coherence and time coherence in random multipath channels," *J. Acoust.Soc. Am.* **62**, 286-294.

[6] Huang S.H., Yang T.C. and Huang C.F., 2013. "Multipath correlations in underwater acoustic communication channels," *J. Acoust. Soc. Am.* **133**, 2180-2190.

[7] Spindel R.C., Porter R.P. and Jaffee R.J., 1974. "Long-range sound fluctuations with drifting hydrophones," *J. Acoust. Soc. Am.* **56**, 440-446.

[8] Williams R.E. and Battestin H.F., 1976. "Time coherence of acoustic signals transmitted over resolved paths in the deep ocean," *J. Acoust. Soc. Am.* **59**, 312-328.

[9] Dyer I., 1987. "Ocean dynamics and acoustic fluctuations in the Fram Strait marginal ice zone," *Science.* **236**, 435-436.

[10] Badiey M., Simmen J. and Forsythe S., 1997. "Frequency dependence of broadband propagation in coastal regions," *J. Acoust. Soc. Am.* **101**, 3361-3370.

[11] Rouseff D. *et al.,* 2002. "Coherence of acoustic modes propagating through shallow water internal waves," *J. Acoust. Soc. Am.* **111**, 1655-1666.

[12] Yang T.C., 2006. "Measurements of temporal coherence of sound transmissions through shallow water," *J. Acoust. Soc. Am.* **120**, 2595-2614.

[13] Siderius M., Porter M.B., Hursky P. and McDonald V., 2007. "Effects of ocean thermocline variability on noncoherent underwater acoustic communications," *J. Acoust. Soc. Am.* **121**, 1895-1908.

[14] Herbers T.H.C., Lowe R.L. and Guza R.T., 1991. "Field verification of acoustic Doppler surface gravity wave measurements. *J. Geophys. Res.,* **96**(9), 17023 -17035.

[15] Hermand J.P. and Roderick W.I., 1988. "Delay-Doppler resolution performance of large time-bandwidth product linear FM signals in a multipath ocean environment," *J. Acoust. Soc. Am.* **84**, 1709-1727.

[16] Hermand J.P. and Roderick W.I., 1993. "Acoustic model-based matched filter processing for fading time-dispersive ocean channels: Theory and experiment," *IEEE J. Ocean. Eng.* **18**(4), 447-465.

The Journal of Acoustical Society of India : Vol. 46, No. 1, 2019 (pp. 28-34)

Design and Development of High Frequency Transducers for Underwater Acoustic Imaging

G. Suresh, A. Shanavas and T. Mukundan
Naval Physical and Oceanographic Laboratory, Kochi-21
e-mail: sureshg@npol.drdo.in

[Received: 01-10-19; Revised: 11-10-19; Accepted: 11-11-19]

ABSTRACT

Imaging systems are used to identify an underwater object by gathering information about its geometrical features, rather than its location. This paper presents the design, fabrication and underwater evaluation of ultrasonic imaging transducer arrays with various configurations: linear 8, 16, 64 & 128 elements that operate at 500 kHz & 1 MHz; Planar transducer arrays with 25, 36, 128 & 169 elements that operate at 500 kHz. Two types of transducer array configurations: Parallel & Mills-cross were developed with 128 elements. The SL and RS of 128 element array are 198.7 dB and -197.4 dB at 500 kHz. The centre 5x5 matrix in the 13x13 array shows a SL of 197.8 dB and RS of 196.98 dB respectively at 500 kHz.

1. INTRODUCTION

Underwater acoustic imaging systems provide images of underwater objects when water turbidity precludes the use of optical means of viewing. Although underwater optical vision provides images with finer resolution with respect to the acoustical one, its range is limited to a few meters in turbid water. Acoustic pictures are different from pictures made from light in that they are essentially maps of density variations. Imaging systems are used to identify an underwater object by gathering information about its geometrical features, rather than its location. These systems operate at higher frequencies and provide shorter imaging ranges and can be used on UUVs or as handheld units for divers.

Acoustic image is a visible representation of the strength of the acoustic backscatter from the object onto a two dimensional image medium, which contain useful information to identify the type/shape of an object. The visibility of an object is related to the contrast, which is a function of the acoustic properties of the object, the background, the medium and the illumination. Sound waves will reflect from boundaries between different materials and carry back information about changes in acoustic impedance and object shape to a sensor. Acoustic cameras have outstanding ability in their visibility even in dark or turbid water. A typical sonar image is obtained by plotting the intensity recorded at the receiver versus time for each beam in a particular azimuth direction. Underwater acoustic imaging systems are useful for either classifying objects or observing the details of objects. These systems are useful in differentiating mines from rocks, coral heads, and garbage on the ocean bottom, and in general, differentiating between objects that warrant further investigation.

This paper presents the design, fabrication and underwater evaluation of ultrasonic transducer arrays of various configurations: (1) linear 8, 16, 64 & 128 elements that operate at 500 kHz & 1 MHz (2) Planar transducer arrays with 25, 36, 128 & 156 elements that operate at 500 kHz. With suitable hardware & software, the acoustic imaging system can be used to image underwater objects in turbid waters along

the estuaries, sea coast and lakes. This system can be used for remote monitoring and surveillance of maritime activities, exploration of the seabed and for UUVs or as handheld camera for divers.

2.. IMPORTANCE OF UNDERWATER ACOUSTIC IMAGING

The challenges of marine exploration and exploitation have highlighted the need for acoustic imaging sonar. With the advent of the war on terrorism, security requirements for the nation's ports and harbours have increased exponentially. A grave threat to ports and harbours are mines or improvised explosive devices placed on ship hulls, piers, berths, and beds of harbours; underwater detection is predominately carried out by divers. In dark, turbid water their searches require slow, tactile examinations. The Navy has a continuing and pressing need to improve its ability to visually detect and identify underwater objects.

Imaging sonar have a number of underwater applications like unmanned undersea vehicles used for improved obstacle avoidance, mine detection and reconnaissance, inspection of underwater power and telecommunication cables, pipelines and navigation. Divers use hand held 3D sonar imaging system for navigation in low visibility conditions, such as in shallow waters, rivers, or ports. Forward-looking 2D acoustic transducer arrays are a promising technology for 3D underwater imaging. Since the beamformer output signal provides information about the structure of a scene in the steering direction, it is possible to create a whole image of the scene by a single illumination and by repeating the beamforming operation after setting many steering directions, as in a raster-scan operation.

3. DESIGN OF IMAGING TRANSDUCER ARRAY

When designing an array for imaging, the factors to be taken into account include the lower and upper frequency limitations, the maximum side lobe level of the array defining its dynamic range, array diameter, measurement distance, spatial resolution and size of the mapping area/object. These quantities are highly interconnected. The design is also based on the geometry, volume fraction, pitch, kerf width, pressure release mechanism, EMI shielding, backing and encapsulation.

As the ultrasound travels through water, it gets attenuated due to spreading, scattering and absorption. The rate of attenuation is proportional to the frequency of ultrasound. Therefore, there is a trade off between resolution and penetration depth. The maximum ranges are limited at the upper frequencies by the attenuation coefficient of seawater and at all frequencies by spherical spreading loss. The depth of field of the imaging system depends on the duration of the acoustic signal, the properties of the acoustic receiver, and the focusing capability of the imaging system. The key parameters describing the performance of transducers are sensitivity, electrical impedance, mechanical impedance, beam pattern, beam width, directivity etc.

In contrast to electromagnetic array imaging, where narrow band signals with wavelengths exceeding the array antenna elements are used, broadband pulsed waveforms are commonly used in acoustic array imaging. The wavelength corresponding to the center frequency of these pulses is often the same size as the array elements. This make diffraction effects apparent resulting in a frequency dependent beam directivity of the array elements.

A 2D imaging sonar consists of an array of transducers arranged in an order that yields the desired illumination of the scene by sound pulses. Two-dimensional imaging sonars operate at high frequencies to provide the desired resolution. The primary task is to form beams on both transmit and receive at a significantly fast rate to enable real-time imaging. The central frequency is determined by a balance between the need to achieve high resolution and the need to avoid strong attenuation in the water. The bandwidth is chosen large enough to give the desired range resolution. The number of elements is chosen to make the distant side lobe level sufficiently small.

The geometry of the narrow sound pulses provides good localization accuracy in azimuth direction. Properly designed transducer can significantly reduce the amount of processing required to form quality

images. A narrower, well defined beam pattern also produces higher definition but reaches a trade off limit with scan coverage requirements restricting the speed of the transducer movement or the scan speed. The beam width characteristics are controlled by the physical characteristics of the transducer. Thus the best compromise to optimize the physical beam forming characteristics are a fairly high frequency in the range between 300 kHz and 900 kHz, a horizontal beam width less than 1° and the shortest pulse length that can effectively produce the desired detection range. Its range of applicability varies according to the specific sensor used or, rather, to the signal frequency characterizing the sensor. Generally, high frequencies are utilized for a visibility range going from centimetres to 100 meters, leaving out all applications specifically devoted to seafloor survey and mapping.

4. DEVELOPMENT OF ACOUSTIC IMAGING TRANSDUCERS

The image enhancement mainly depends on the quality of the original echo signal, making the transducer the most critical components of imaging system. By using time delays in the electrical activation of the discrete elements across the face of the transducer, the ultrasound beam can be steered and focused electronically for creating the image. The major challenge in the realisation of transducers for imaging applications is to obtain narrower beams with very high sensitivity and low side-lobe levels.

The imaging transducer arrays were fabricated using 1-3 piezo composite elements with identical electrical characteristics. 1-3 piezo composite sensor consists of piezo pillars embedded in a polymer matrix. The principal advantages of the piezo composites include higher coupling in the thickness mode, lower mechanical impedance, reduced lateral mode interference, and better electrical load matching, increased sensitivity, better resolution by broader bandwidth, improved image contrast, better efficiency, greater element to element phase and amplitude uniformity, achieved by selectively patterning the signal electrodes on the composite pillars defining the array elements[1,2].

The interconnection between array elements and system electronics is a critical and challenging step in the high-frequency array fabrication process. Because of the fine element spacing, techniques such as traditional soldering or bump bonding connections from elements to more coarsely spaced system circuitry are not practical. A proprietary interface FRP structure device is developed for reliable interconnection between the sensor elements and the coaxial cable assembly. The rectangular elements as used in linear arrays produce elliptical beams and hence the lateral resolution is better in one plane of the beam than the other.

The projector is developed for a central frequency of 500 kHz, a frequency that can guarantee both a high resolution of the image and a good visibility range. The receiver is composed by an array of sensor elements, electrically and mechanically insulated. The transducer parameters were optimised for better performance & resolution. The projector and receiver arrays with high impedance backing were encapsulated. It provides waterproofing and acoustic matching to control and enhance the bandwidth of the transducer and for improved output levels.

4.1 Development of Linear transducer arrays

The transducer array consists of the piezoelectric material, matching layer, backing block, acoustic absorber, insulating cover, sensor electrodes, and transducer housing. The matching layer with proper acoustic impedance provides improved transmission and reception of the ultrasound echoes. The backing material provides high attenuation and match with the acoustic impedance of the piezoelectric material for efficient coupling. Designed and fabricated linear underwater transducer arrays of various configurations - 8, 16, 64 & 128 rectangular elements using 1-3 piezo composites operating at 500 kHz & 1 MHz (Fig. 1).

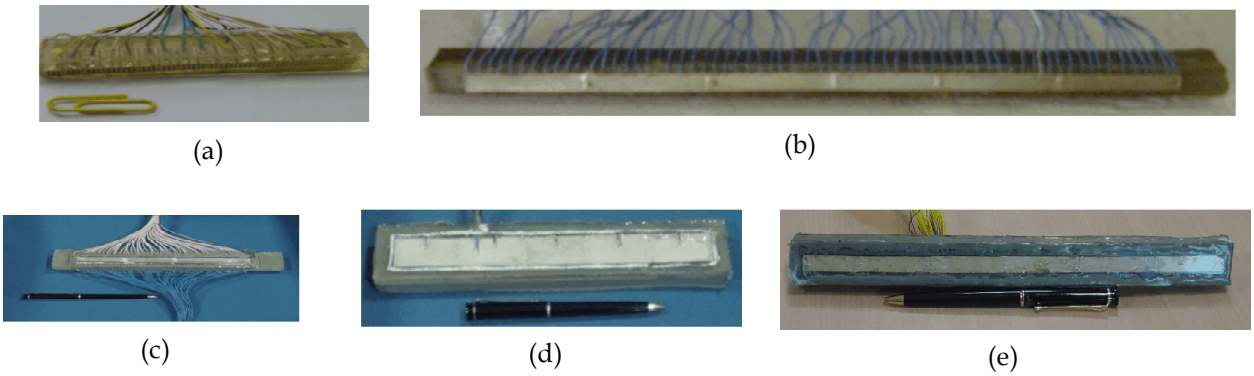

Fig. 1: (a) 16 Element linear array at 500 kHz (9×1.5×1 cm); (b) 64 Element linear array at 500 kHz (21×1.5×1 cm); (c) 128 Element linear array at 500 kHz (26×2×1 cm); (d) Transmitter array for 500 kHz (28×2×1 cm); (e) 128 Element linear array at 1 MHz

Two types of front end configurations - Parallel & Mills cross of the transducer were attempted with the developed 128 elements 500 kHz/1MHz transmitter & receiver arrays. A vertical transmitting array insonifies a thin slice in elevation, then a horizontal receiving array collects the signals from different azimuth angles across each emitted slice. This arrangement (Fig. 2) is the "Mill's Cross Configuration"; its main advantage is the small number of transducers and transceiver channels.

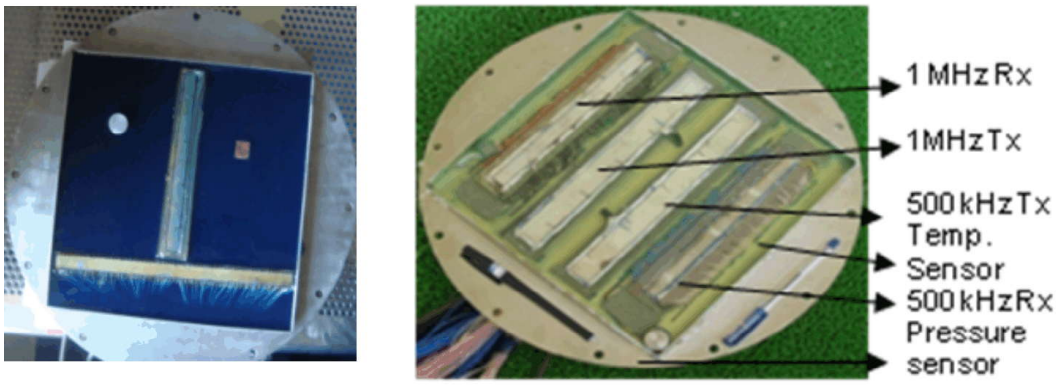

Fig. 2: Transducer array with (a) Mill's cross configuration; (b) Planar configuration

Evaluated the linear transducer arrays in the pulse-echo mode in underwater for its transmittance and receiving characteristics. Each array element is characterized for the frequency response, capacitance, impedance and inter-element cross coupling to ensure the identical response of the array elements. A high frequency acoustic calibration facility developed at NPOL (Fig.3) is used for the calibration and testing of high frequency transducer arrays. It has linear positioning system - software controlled for translation along X, Y and Z axes (±1 mm) and rotational modes (0.2 degree) of evaluation that can be operated in both auto and manual modes.

An acoustic water tank of dimension 3 x 1.5 x 1.5 m which has two trolley supports which can move along length of the tank for transducer positioning. The linear response of transmitter and beam width of each transducer element (Fig. 4) was measured using the linear positioning system. The Source Level and Receiving Sensitivity of the 128 element linear arrays are: 198.7 dB & -197.4 dB at 500 kHz and 172 dB & -212 dB at 1 MHz (Table. 1).

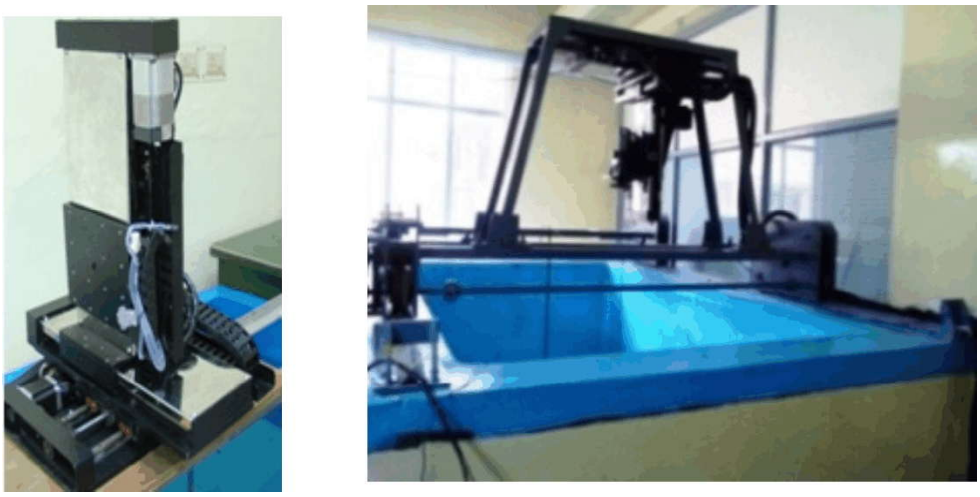

Fig. 3: (a) Linear Positioning System; (b) Measurement water tank

The 500 kHz array has a single element beam width of 0.80. The cross-talk of all the sensor arrays was measured underwater and is less than -25 dB.

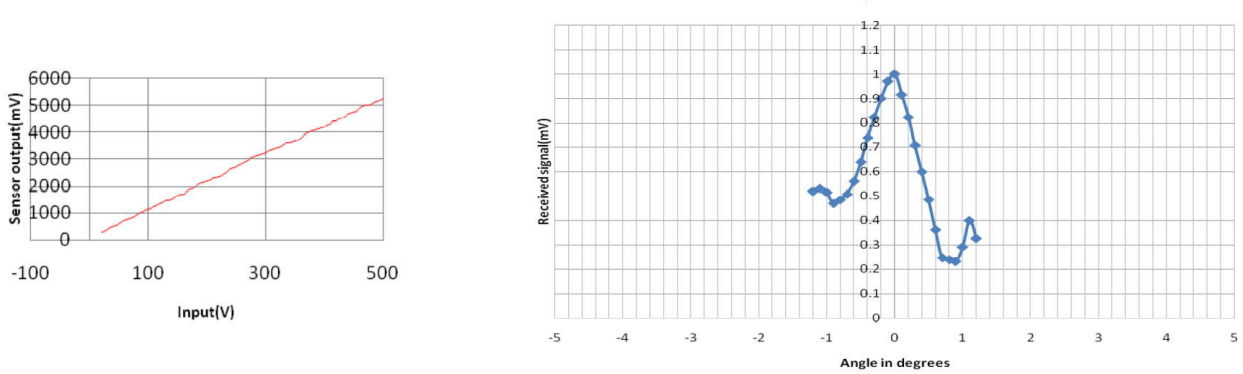

Fig. 4: (a) Transmission characteristics and (b) Beam width of sensor element at 500 kHz

4.2 Development of 2D Imaging Transducers

The designing of planar array is turned into an optimization problem to reduce the number of acoustic sensors, to find optimum positions and weights for the sensors, to lower the side lobe level, narrow the main lobe width, and to avoid grating lobe in the beam pattern.

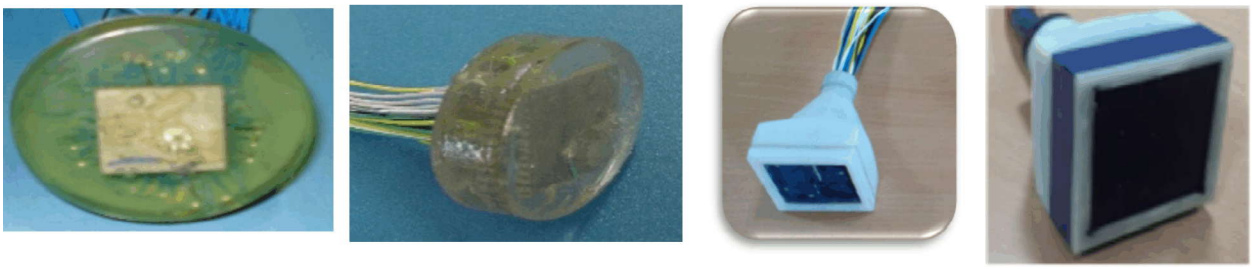

Fig. 5: (a) 5×5 sensor array (1.8 × 1.8 cm); (b) 6×6 sensor array (1.8 × 1.8 cm);
(c) 128 Element 2Darray (6.2 × 6.2 cm); (d) 169 element 2D array (6.2 × 6.2 cm)

Planar transducer arrays with transducer matrix 5×5, 6×6, 12×12 and 13×13 (Fig. 5) were designed, fabricated and evaluated underwater. All elements were characterized for frequency response, capacitance, impedance (Fig. 6) *etc*. to ensure identical response of array elements.

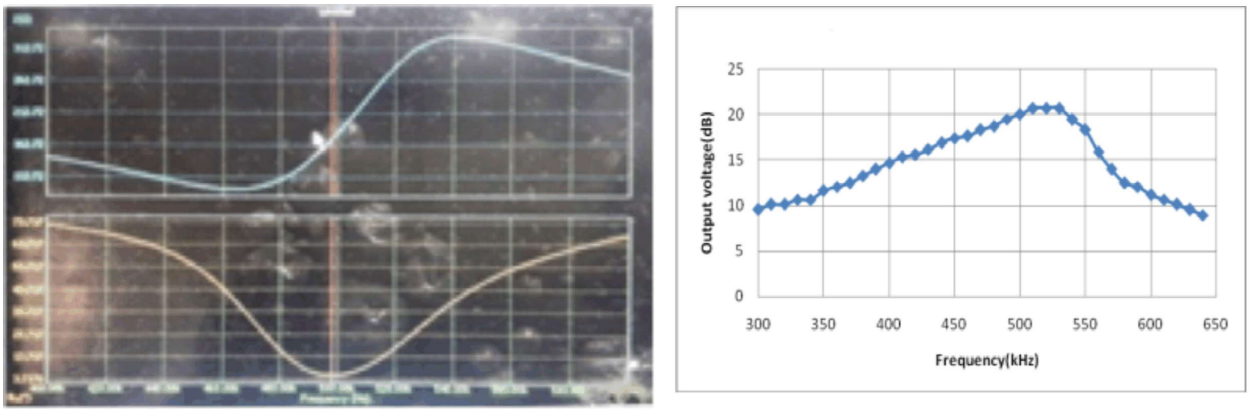

Fig. 6: (a) Impedance Spectra of an element in the array;
(b) Frequency response of 2D array element at 500 kHz

The 13×13 matrix transducer consists of 169 individual rectangular piezo electric elements, which can suitably configure the number of elements for transmit and receive acoustic signals of 500 kHz frequency. The arrays are evaluated underwater using pulse-echo method at far-field free-field region for transmitting and receiving characteristics (Table 1).

Table 1: Underwater acoustic measurement results

Parameter	**64 element 1DArray**	**128 element 1DArray**	**128 element 2D Array**			**128 el ement 2D Array**
No. of elements	Single element	Single element	Single element	Two elements	4 x 4 elements	Single element
Frequency	500 kHz	500 kHz	500 kHz	500 kHz	500 kHz	1MHz
Receiving sensitivity (dB reV/µPa)	-207.5	-197.3	-190.6	-189.9	-189.6	-212 dB
Source level (dB re µPa/V)	190.2	198.6	155.8	179.4	190.6	172 dB
TVR (dB re µPa/V)	156.3	153.7	126.4	149.9	161	137.6 dB
Acoustic cross talk(dB)	< -20	< -25	< -25	< -25	< -25	< -25

5. CONCLUSION

Underwater imaging transducer arrays with linear and planar configurations operate at 500 kHz were designed and developed using 1-3 piezo composites. Two types of transducer array configurations: Parallel & Mills-cross were developed with 128 element transducer arrays operating at 500 kHz & 1 MHz.

Developed 2D transducer arrays with 128 & 169 individual rectangular piezo electric elements, which can transmit and receive acoustic signals of 500 kHz frequency. The SL and RS of the centre 5x5 element array at 500 kHz is 197.8 dB and -196.9 dB, respectively.

6. ACKNOWLEDGEMENTS

The authors thank Director, NPOL for the encouragement and permission to publish this work and NMRL for providing the piezocomposites.

7. REFERENCES

[1] S. Cochran Microscale, P. Marin-Franch Microscale, D. Choi, Z. Wu, M.P. Walsh, M. Parker Microscale and K.J. Kirk Microscale, 2005. "Present and future piezocomposite technology in underwater sonar transducers,", **27**, Pt. 1.

[2] Thomas R. Howrah, 2000. "Electroacoustic evaluations of 1-3 piezocomposite Sonopanel materials," *IEEE Transactions on Ultrasonics, Ferroelectrics and Frequency Control*, **47**(4).

The Journal of Acoustical Society of India : Vol. 46, No. 1, 2019 (pp. 35-43)

Battery Operated Power Amplifier for Underwater Sensor Networks

V. N. Panchalai, Yateesh Kumar Mishra and Jeffin George
Naval Physical and Oceanographic Laboratory,
Thrikkakara, Kochi, India-682021
e-mail: panchalai@gmail.com

[Received: 01-10-19; Revised: 11-10-19; Accepted: 11-11-19]

ABSTRACT

Underwater Sensor Networks (USN) are deployed to study the oceanographic parameters wherein the monitored parameters are processed and modulated before acoustically transmitting underwater. The transmitted acoustic signal is received at receiver end and then demodulated to retrieve the parameters. The transmitter uses Power Amplifier (PA) to amplify modulated signals. PA excites electroacoustic transducer with amplified signal. A battery powered PA which can be used in transmitter of USN is explained in this paper. A boost converter is designed to step up the battery voltage before connecting it to the PA. Applications of this system include underwater echo repeaters, underwater acoustic measurements and underwater acoustic modem. This system is advantageous in terms of cost, space and unmanned operation. Salient results of prototype hardware are presented.

1. INTRODUCTION

Underwater Sensor Networks (USN) are used to measure oceanographic parameters for longer duration and also to monitor underwater threats. Power Amplifiers (PA) are used in acoustic modem of USN to excite the electro acoustic transducers with modulated signals. Different modulation techniques are used at transmitter end and demodulated at receiver end. The modulated signal needs to be amplified with least distortion so that it is received and demodulated without error at the receiver end. There are many modulation techniques such as Binary-Phase-Shift-Keying (BPSK), Quadrature Phase Shift Keying QPSK, ON-OFF Keying, Frequency Shift Keying (FSK), etc. are used in underwater communication. The modulated signal contains multiple frequency components and hence linear class-A or class-AB PA are generally the preferred choice as they amplify the input signal with least distortion. The PA for USN are operated using portable power sources like Batteries, less efficient PA classes such as class-A, class-AB will drain the power source faster.

M. Aydinlik *et al.*[1] used class-B PA in underwater acoustic modem and reduced power consumption by switching PA off when not in use. Class-AB PA is modified in A. Sanchez *et al.*[2] as digitally controlled push-pull class-B power amplifier. The transmitted power was around 2W and it uses transistor as power switch. Switch Mode Power Amplifiers (SMPA) are better choice in efficiency point of view but with distortion at the output. However, a careful design of SMPA can have better efficiency as well as acceptable distortion. The USN required to be operated for longer duration, high efficiency PA is very much essential. So SMPA are used in many systems[3, 4, 5]. Advantages of SMPA for underwater modem is explained in ref[6]. It used class-D PWM amplifier for Orthogonal Frequency-Division Multiplexing (OFDM)

transmissions and a digital controller to generate the PWM signals. B. Benson *et al.*[7] used class AB amplifier coupled with current controlled class-D amplifier for the improvement of efficiency as well as to improve the quality of the transmitted waveform.

In this paper a battery operated SMPA that operates in the frequency range from 5 kHz to 30 kHz which can also be used for voice communication is explained. A high efficiency boost type DC-DC converter is connected between class-D SMPA and battery. It regulates the input to SMPA at a constant voltage so that the output of SMPA is maintained at selected value.

2.. POWER AMPLIFIER FOR UNDERWATER ACOUSTIC MODEM

Typical underwater transmitter consists of a signal generator, a PA and an acoustic projector. The signal can be generated either using analog methods or using digital processors. The modulated signal from signal generator is then given to PA for further amplification and excitation of the acoustic projector.

Proposed boost converter fed SMPA is shown in Fig. 1 and its subsystems are explained in this section.

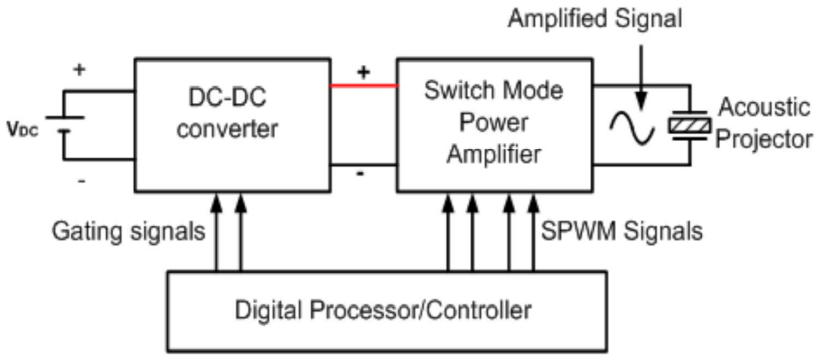

Fig. 1: Block schematic of proposed SMPA

2.1 Battery (VDC)

The duration of USN deployment depends on the capacity of the battery. Lithium based batteries have higher volumetric energy density[8-9]. Rechargeable batteries have less volumetric density than primary cells but they can be reused after recharging. The recharging can be done by energy harvested under water. Primary batteries are the better choice for the deployments of single use.

2.2 DC-DC converter

The DC-DC converter acts as an interface between the battery and SMPA. The output of DC-DC converter is regulated so that the SMPA delivers required output even when battery discharges. Non isolated boost is chosen considering the requirement of voltage boost and high efficiency. This converter doesn't require additional isolated supply for driving power device. Another advantage of the converter is that the current drawn will have the switching frequency of the boost converter which is very high compared to the signal frequency and the ripple is also less.

2.3 SMPA

The class-D SMPA is proposed in system. The power devices in the SMPA are operated at carrier frequency which is much higher than the signal frequency. This limits the maximum frequency of the signal that can be amplified. However, SMPA can be designed to operate frequencies up to 30 kHz without compromising efficiency and THD[10]. Multilevel topology of switch mode technology is a good option at higher frequencies[11] with acceptable increase in THD. The power rating of SMPA depends on the Source Level (SL) requirement of the system. The SL can be expressed[12-13] as

$$SL = 170.8 + 10\ log_{10}\ P_e + 10\ log_{10}\ (\eta) + DI \quad (1)$$

where, 'DI' is the Directivity Index, 'Pe' is the electrical power applied to the projector and η is the conversion efficiency. Based on the range requirement, Pe is chosen and the SMPA design is carried out.

Unipolar Sine Pulse Width Modulation (USPWM) is used as gate signals for the Controlled Full Bridge (CFB). The output of the CFB has the harmonic frequency which is twice the switching frequency. Advantages of USPWM are

1. The filtering becomes easy with smaller filter components and hence distortion becomes less.
2. The carrier frequency for USPWM can be chosen lower so that the effective filtering still be possible which extends the maximum operating frequency of the power amplifier.

2. 4. Acoustic Projector

The equivalent circuit of typical acoustic projector with single resonance consisting of reactive components[12-13] is given in Fig. 2 where Co is the clamped capacitance due to the dielectric constant of the piezoelectric material, R1, L1 and C1 correspond to the motional part of a resonance mode.

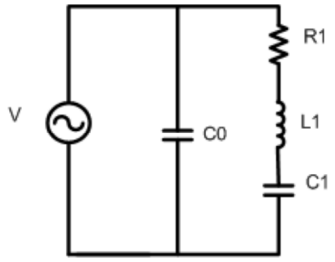

Fig. 2: The equivalent circuit of typical electro acoustic transducer

The impedance of the transducer is a complex parameter and it varies with the frequency. So the impedance and phase offered to the PA varies with the frequency. This puts the limitation on the bandwidth of the usage. Broadband tuning is an option to improve the bandwidth of PA[14].

2. 5. Digital Processor and controller

The functional requirement of the digital controller in SMPA are

(a) Generation of gating signal for boost type DC-DC converter
(b) Generation of USPWM signals for SMPA
(c) Control of timings of the acoustic transmission
(d Feedback control to tackle the variation in the battery voltage due to discharge and the change in impedance due to the change in transmit frequency.

There are many digital controllers available in the market which can meet the above requirements.

3. DESIGN OF BOOST CONVERTER AND SMPA

Control circuitry and processor for the proposed system use voltages such as 3.3V, 5V or 12V. These voltages are to be derived from the battery. Lithium ion batteries can be configured to supply a voltage between 12V to 16.8V with a nominal voltage of 14.8V. The electroacoustic transducer requires hundreds of volts to achieve required source level. So a step-up transformer is used. Schematic of the proposed boost converter fed SMPA is shown in Fig. 3.

Components L1, S1, D1 and C1 forms a boost converter whose input and output voltage are related by equation (2)

$$V_0 = \frac{V_{in}}{1-D} \tag{2}$$

where the Vin is the battery voltage, Vo is the voltage across capacitor C1 and D is the duty ratio of the switch S1. The duty ratio D is defined as the ratio of switch ON time to total period. The value of D is such that $0 \le D \le 1$. MOSFETs S2 to S5 form a CFB converter. The gates of S2 to S5 are driven by the USPWM signals which are generated by digital controller[10]. Centre tapped full bridge is the better topology in efficiency point of view. CFB with USPWM has the advantage of lesser distortion as the harmonic content of the output voltage has the twice the switching frequency of device. However, the choice is based on the requirement and compromise between the efficiency and distortion. The Power transformer is designed to operate in the frequency band of interest. L2 and C2 form low pass power filter which removes the harmonic contents present at the output of transformer secondary.

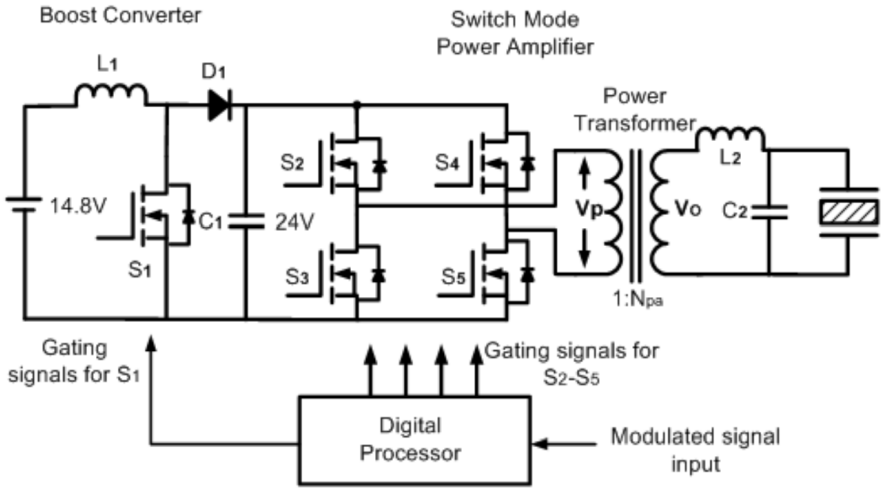

Fig. 3: Schematic of proposed power amplifier

4. PROTOTYPE AND RESULTS

A 50W prototype was developed whose specifications are given in Table 1.

Table 1: Prototype parameters

Sl. No	Description of the parameter	Parameter Value
1	Battery Voltage	14.8 V Nominal
2	Min. Battery Voltage	12.0 V
3	Max. Battery Voltage	16.8V
4	Boost Converter Output	24 V
5	PA Output Power	50 W
6	Operating Frequency Range	5 kHz to 30 kHz

Fig. 4(a) & 4(b) show the gating signal of MOSFET S1 and the boost converter's output voltage when battery voltage is maximum (16.8V) and minimum (12V) respectively. It can be observed that the converter output is constant with input voltage varying. The pulse width of the gating signal is modified by taking a feedback from the boost converter output voltage.

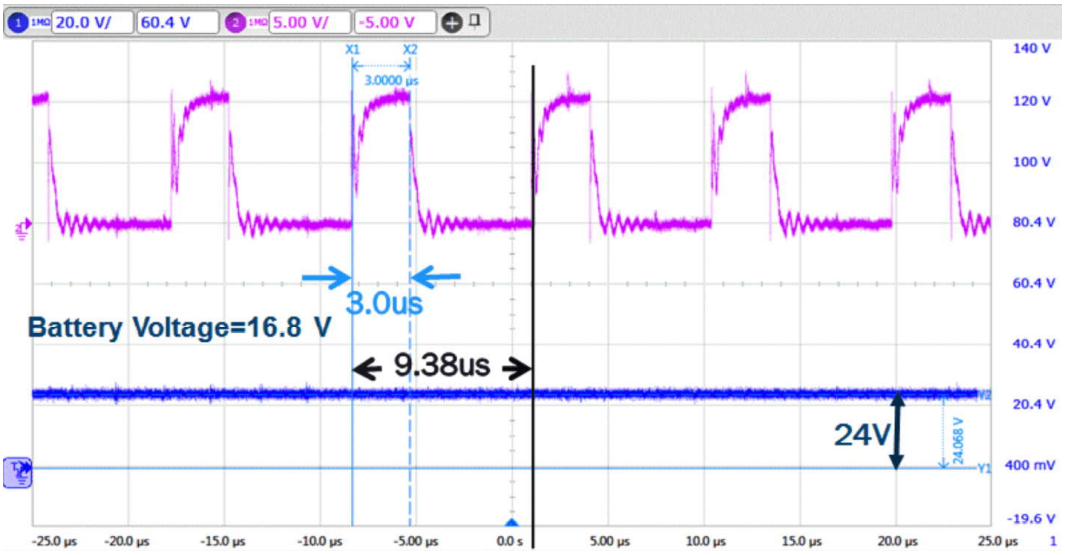

Fig. 4: (a) Gating signal of S1 in boost converter when battery is fully charged (16.8V)

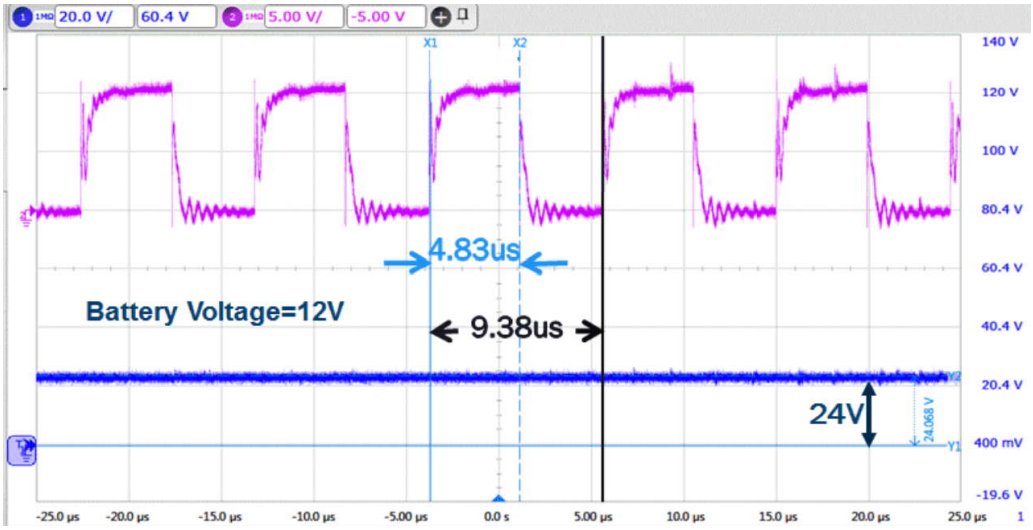

Fig. 4: (b) Gating signal of S1 in boost converter when battery is fully discharged (12V)

The SMPA uses MOSFET based CFB circuit. MOSFET with low RDS-ON is chosen for CFB to reduce the conduction losses. The carrier frequency of the MOSFET is chosen to be 180 kHz. The generation of USPWM is implemented using digital controller dsPIC30F2010. Digitally generated USPWM is shown in Fig. 5. Inbuilt PWM module of digital controller is configured to give USPWM signal corresponding to modulated signal.

Waveforms marked 1 and 2 are used to drive high side devices S2 and S4 respectively. Low side devices S3 and S5 are driven with the complementary signals of S2 and S4 respectively. A dead time is inserted between gate signals of S2 and S3 (as well as S4 and S5) to avoid shoot through. The output of CFB is isolated using an isolation transformer followed by filtering operation with a low pass filter (L2

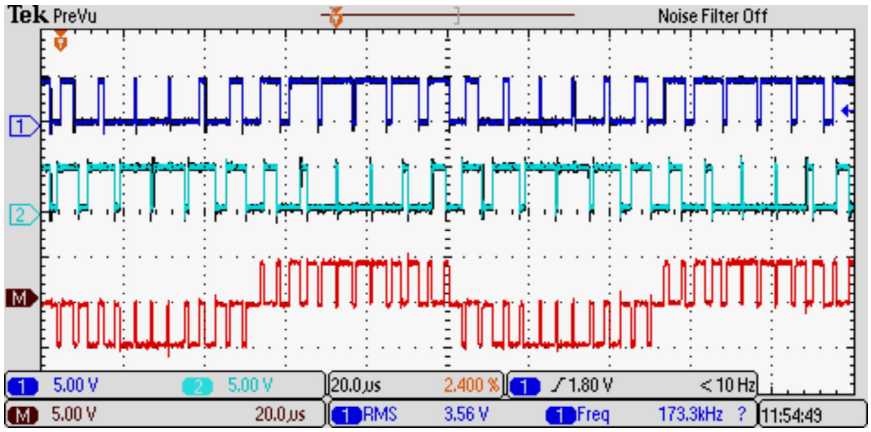

Fig. 5: Snapshot of USPWM signals for gates of (S2 and S4)

and C2). For a typical value of 200 ohms impedance of the acoustic projector, 100V is expected across the projector for 50W power output. With 24V as input to the CFB, the transformer turns ratio should be approximately 1: 5. The output of the filter is amplified version of modulated signal which is used to drive the acoustic projector. Typical output waveform and its FFT are shown in Fig. 6. It can be observed from the FFT that the harmonic content is very less which indicates the minimum distortion in the output waveform.

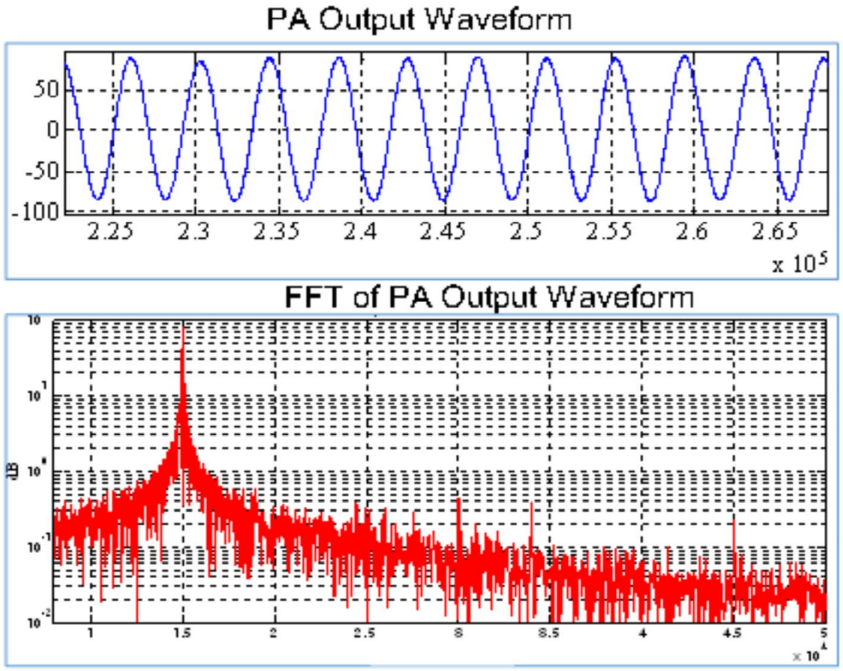

Fig. 6: PA output waveform and its FFT

To verify the bandwidth of the system, USPWM for a typical Linear Frequency Modulated (LFM) signal of 10 kHz to 20 kHz was generated, and amplified. The input signal, its FFT, SMPA output and its FFT are shown in Fig. 7. It is observed that the output waveform is amplified version of input with very less distortion which can be witnessed from their FFTs also.

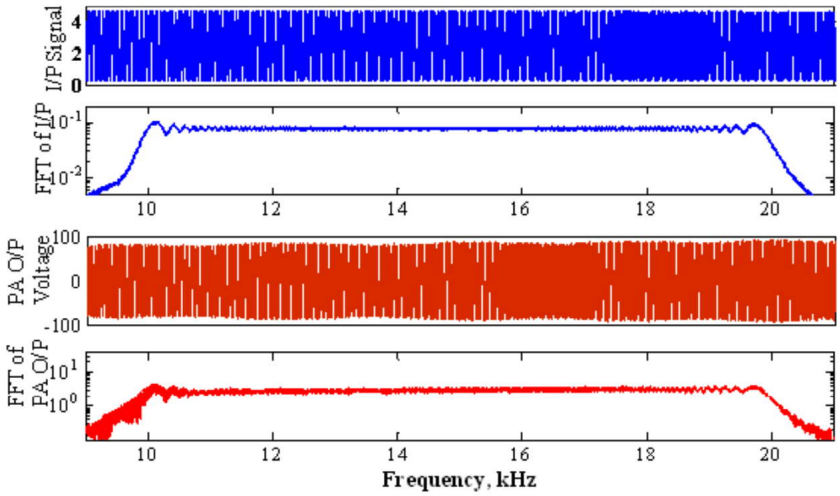

Fig. 7: Input signal with FFT and output of SMPA with its FFT

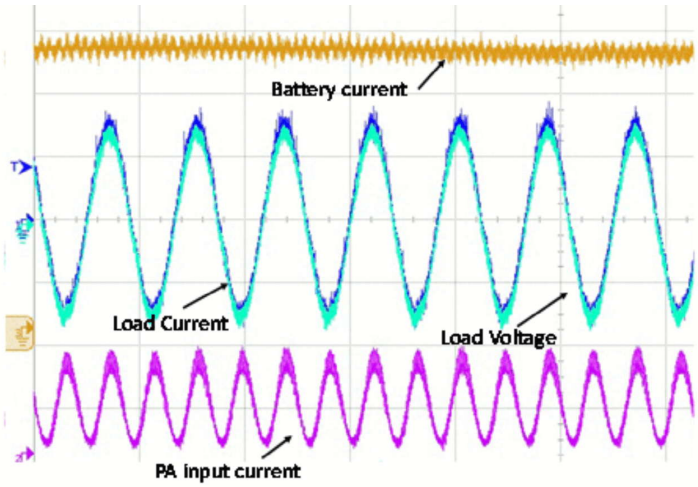

Fig. 8: Different waveforms of the system with resistive load

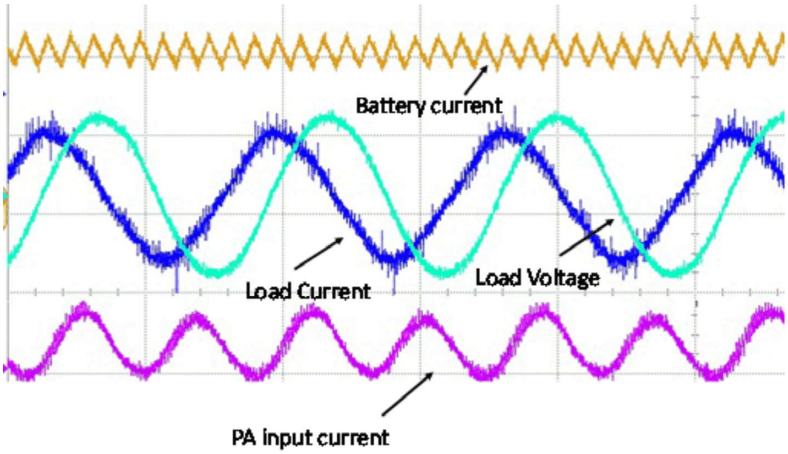

Fig. 9: Different waveforms of the system with resistive load

Another important characteristic of this system is that the amplitude of SMPA's output is same for a particular input signal even when the battery voltage gets reduced due to discharge. The SMPA output voltage, output current, battery current and PA input current with resistive load and reactive load are shown in Fig. 8 and Fig. 9 respectively.

The battery current has high frequency ripple and amplitude of the battery current for both resistive load and reactive load is more or less same. This shows that the battery current doesn't get affected by the power factor of the load. This is very much beneficial for the applications like underwater transmissions where the transducer load impedance and phase depends on the drive frequency. Since the bandwidth is a key parameter in underwater communication systems, the impedance and phase variation is inevitable. The load will be resistive at its resonance frequency and reactive on either side of the resonance frequency. This will impose low frequency ripple current which is not good for the battery. The boost converter isolates the low frequency ripple current generated due to the load impedance from the battery. This can be observed from Fig. 8 and Fig. 9. The power amplifier input current ripple which has the twice the frequency of load current is not reflected at the battery. The boost converter is realized with single switch and its practical efficiency achieved is around 95%. Practical efficiency of SMPA is around 85%. The system was tested with different modulation techniques and the performance of the system was satisfactory.

5. CONCLUSION

Battery operated power amplifier is an important subsystem in USN. A battery operated SMPA which can be used for acoustic modem is explained. A boost type DC-DC converter is connected between battery and SMPA. The boost converter regulates the input voltage to SMPA and does not pass the low frequency ripple current to the battery. Digital controllers were used to control the boost converter as well as the SMPA. SMPA uses USPWM which has advantage in terms of harmonic frequency that makes the filter components small. A prototype design of the system and results are presented.

6. REFERENCES

[1] M. Aydinlink, A. Turan Ozdemir and M. Stojanovic, 2008. "A Physical layer implementation on Reconfigurable Underwater Acoustic Modem," In Proc. of OCEANS 2008, pp. 1-4.

[2] A. Sanchez S. Blanc, P. Yuste and J.J. Serrano, 2011. "A Low Cost and High Efficient Acoustic Modem for Underwater Sensor Networks," In Proc. of OCEANS 2011, *IEEE,* pp. 1-10.

[3] L. Freitag, M. Grund, S. Singh, J. Partan, P. Koski and K. Ball, 2005. "The WHOI Micro-Modem: An Acoustic Communications and Navigation System for Multiple Platforms," In Proc. of OCEANS 2005, *IEEE,* pp. 1086-1092.

[4] Ronald A. Iltis, Hua Lee and Ryan Kastner, 2005. "An underwater acoustic telemetry modem for eco-sensing," In Proc. of OCEANS 2005, *IEEE,* pp. 1844-1850.

[5] J Wills, W. Ye and J. Heidemann, 2006. "Low-power acoustic modem for dense underwater sensor networks," In Proc. of the 1st ACM international workshop on underwater networks, pp. 79-85.

[6] H. Zhou, X. Xu, L. Wei, S. Zhou and J.H. Cui, 2015. "A study on pulse-width-modulation-based power amplification for underwater acoustic OFDM," *IEEE J. Oceanic Eng.* **41**(3), 656-669.

[7] B. Benson, Y. Li, R. Kastner, B. Faunce, K. Domond, D. Kimball and C. Schurgers, 2010. "Design of a low-cost, underwater acoustic modem for short-range sensor networks," In Proc. of OCEANS 2010, pp. 1-9.

[8] S. Specht, 1987. "Advanced batteries for electrically powered underwater vehicles," In Proc. of the 5th International Symposium on Unmanned Untethered Submersible Technology, *IEEE,* **5**, 141-158.

[9] O. Hasvold, N.J. Størkersen, S. Forseth and T. Lian, 2006. "Power sources for autonomous underwater vehicles," *J. Power Sources* **162**(2), 935-942.

[10] V.N. Panchalai, B.P. Chacko and N. Sivakumar, 2016. "Digitally controlled power amplifier for underwater electro acoustic transducers," In Proc. of Signal Processing and Integrated Networks (SPIN) 2016, *IEEE,* pp. 306-311.

[11] V.N. Panchalai and N. Sivakumar, 2016. "Recent trends in power amplifiers for sonar projectors," *J. Acoust. Soc. India* **43**(4), 214-224.

[12] D. Stansfield, 1990. "Underwater electroacoustic transducers", Bath University Press 1990.

[13] R. Ramesh, S.S. Pillai, P. Abraham and D.D. Ebenezer, 2009. "Characteristics of broadband underwater transducers integrated with tuning coils and cable," International Symposium on Ocean Electronics (SYMPOL) 2009, pp. 133-138.

[14] C.H. Chou, J.E. Bowers, A.R. Selfridge, B.T. Khuri-Yakub and G.S. Kino, 1980. "The design of broadband and efficient acoustic wave transducers," Ultrasonics Symposium, *IEEE,* pp. 984-988.

The Journal of Acoustical Society of India : Vol. 46, No. 1, 2019 (pp. 44-50)

Ethernet and High Voltage DC over Single Core Coaxial Cable for High Frequency Applications

Manoj G., Sona O Kundukulam, Biju Gopal and Unikkat Ganesan
Naval Physical and Oceanographic Laboratory, Thrikkakara, Kochi, India
e-mail: manojg@npol.drdo.in

[Received: 01-10-19; Revised: 05-11-19; Accepted: 11-11-19]

ABSTRACT

Coaxial cable telemetry has wide applications such as Airborne Sonar, High frequency Imaging sonar, underwater modem, underwater communications, Active Sonobuoy etc. Handling of high voltage DC and high speed Ethernet over Coaxial (EoC) data through single core coaxial cable is possible using proper coupling schemes. There are several power line communication standards mainly driven by home networking and smart grid requirements. IEEE 1901(IEEE Std 1901-2010) and G.Hn (ITUT G.9960 and G.9961) standards are developed for multimedia access and smart grid applications through power lines. A telemetry scheme with IEEE 1901, which is a recent standard and more robust, that can be able to handle high speed data. The telemetry is named as Ethernet over Coaxial (EoC) and that can transmit the Ethernet data over coaxial cable. For most of the cable telemetry, DC and high speed EoC data are transmitted through multi core cable. Passive Coupling scheme for coaxial cable telemetry over high voltage DC along with EoC data is explained in this paper. In this paper, a passive filter based coupling scheme concept is used to super impose high voltage DC and high speed EoC data. For the sonar applications, it is essential to send high voltage DC and high speed EoC data send across the coaxial cable. The simulation of coupling scheme using Multisim, PSpice® and Matlab Simulink is explained and simulation as well as measurements with prototype board results is discussed.

1. INTRODUCTION

Passive component based coupling schemes are commonly used in power line communication to couple communication data and high voltage. Passive couplers filter out the unwanted band of frequencies so that, the same can be used to implement the passive filter based coupling schemes to super impose EOC data and high voltage DC. Fig. 1 shows the block diagram of coaxial cable telemetry with DC and high speed EoC data. Coupling scheme has wide applications in the field of airborne sonar telemetry[1], high frequency imaging sonar telemetry[2], underwater modem, under water communications, active sonobuoy *etc.* Multi core coaxial cable telemetries are commonly used in all the above applications. High voltage DC and high speed EoC data is required at the remote side and high speed EoC data for onboard side. Multicore cable is not economic and also has engineering challenges. For handling all the signals, proper coupling schemes are essential so that we can use single core coaxial cable. The two types of coupling schemes for coaxial cable telemetry are relay based coupling and passive filter based coupling[3, 4]. To realize telemetry, the coupling network is to be put at both end of the coaxial cable (onboard and remote). At the onboard side, the high speed EoC data and high voltage DC is coupled to the coaxial cable with proper coupler, leads to the superimposition of all the signals in the cable. At the remote side, these are separated out using passive couplers. The challenges of the coupling schemes have already discussed[4].

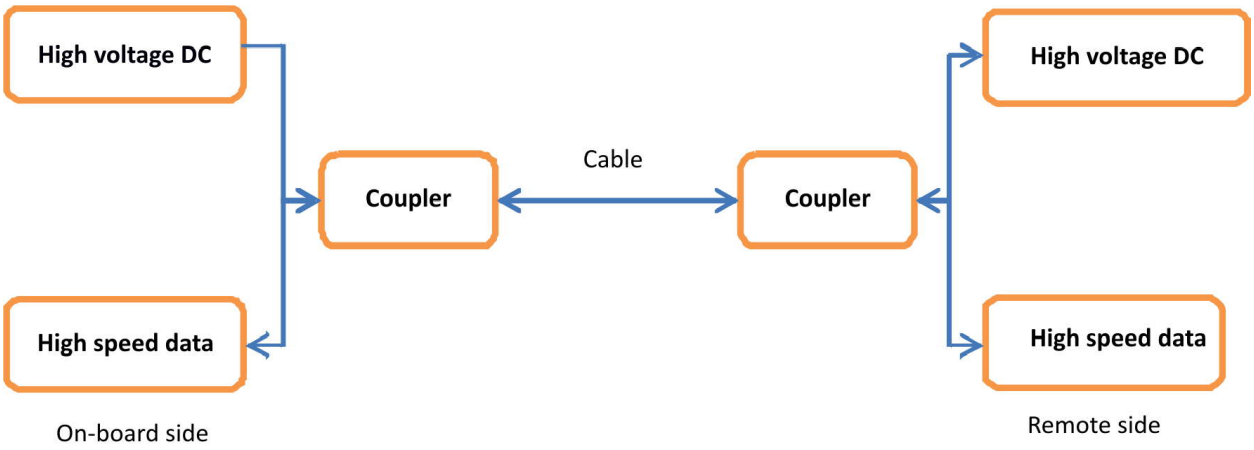

Fig. 1: Block diagram of coaxial cable coupling

2. COUPLING SCHEMES

To realize telemetry for the above discussed applications, it requires a high speed EoC data and high voltage DC. A coupling scheme is to be designed to couple both high voltage DC and high speed EoC data for single core coaxial cable. As the signals are well separated, passive filters are easy to design. Multicore cable are commonly used in this applications. Fig. 2 shows the block diagram of the passive filter based coupling schemes.

The high voltage DC is in the range up to 300V and the data rate of Ethernet is 100Mbps. The Ethernet over coaxial converter converts the Ethernet signals to analog signal and drives over the coaxial cable. The high voltage DC and high speed EoC data signals are well separated band of frequencies.

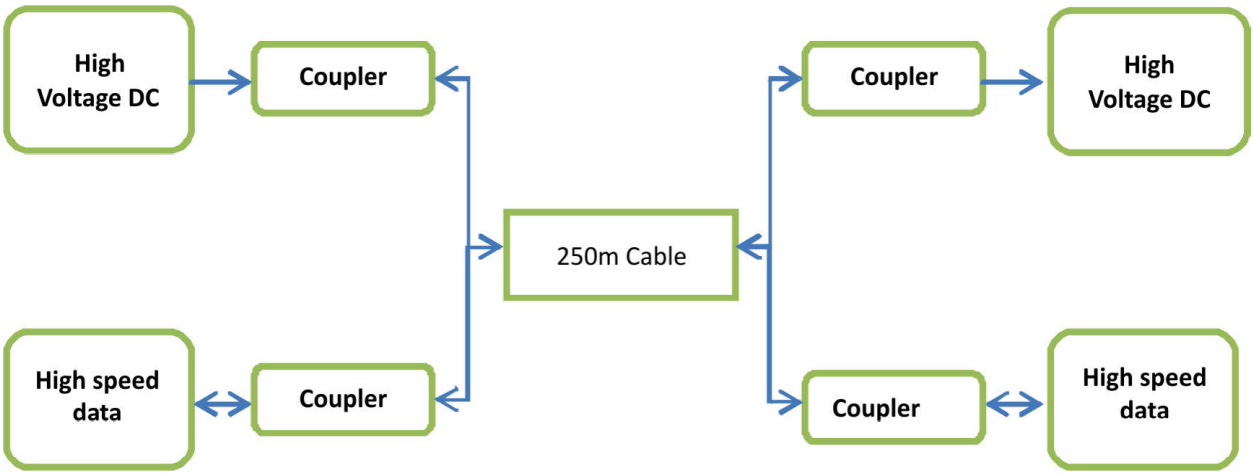

Fig. 2: Block diagram of Passive filter based coupling scheme

3. SIMULATION OF PASSIVE FILTER BASED COUPLING

The Simulation was carried out in Multisim, PSpice® and Matlab Simulink. Analyses were done with and without coaxial cable model. Fig. 3 show the simulation circuit of the passive filter based coupling

scheme without cable model. L1, L2 and L4, L5 is the high voltage DC coupler at the onboard and remote unit respectively. C1, C2 and L3 form the EoC data coupler at the onboard unit and C3, C4 and L6 forms the EoC data coupler at the remote unit.

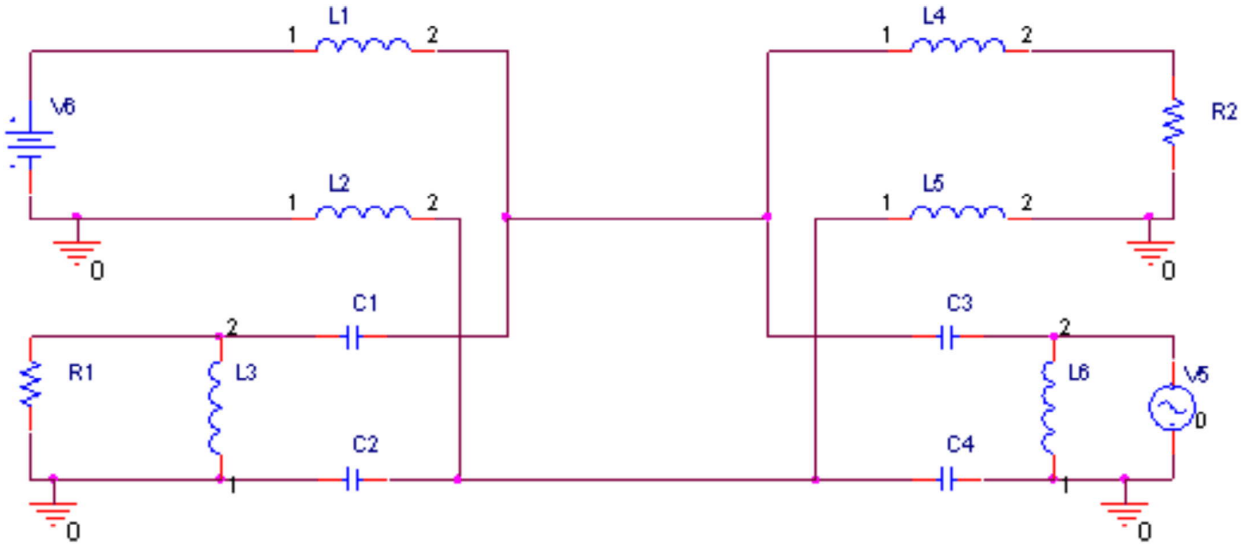

Fig. 3: Simulation schematic of passive coupling scheme

For realizing the single core coaxial cable telemetry, it need to transmit high voltage DC to remote side and high speed EoC data transmit to onboard as well as remote side. As the high speed data and DC are coupled thorugh the single core coaxial cable, it is essential to study the effect of high voltage DC in other coupling paths i.e. On-board data coupler, remote DC coupler and remote data coupler.

The study has carried with and without cable model. The cable model is similar to transmission line model. The values of R, L, C, and G are 33ohm, 1mH, 36nF and 100 Mohm respectively. Analyses were carried out over fixed load resistance R1 and R2. This is the measured values of a single core coaxial cable.

4. MEASUREMENT AND ANALYSIS USING SIMULATION

Designs were simulated on Multisim tool and the frequency responses of the passive filters were plotted. Simulations were carried out with and without single core coaxial cable model to find leakage of high voltage DC and high speed EoC data in each of the coupling paths on both onboard and remote side.

4.1 Filter response

Fig. 4 and Fig. 5 shown below are the frequency responses of the high voltage DC coupler and high speed data coupler. Response has taken for frequency ranges from 0 to 100MHz. Fig. 4 shows the frequency response of high voltage DC coupler. For DC coupler the filter response is low pass and the -3dB point of the high voltage DC coupler comes in the frequency of 13Hz. Fig. 5 is the high speed data coupler and the frequency response is high pass. The -3dB points of the above couplers are318 KHz.

The signals above 10 MHz at the remote side high voltage DC coupler have an attenuation of-234dB. Similarly the attenuation of DC component at the onboard data coupler is -422dB.

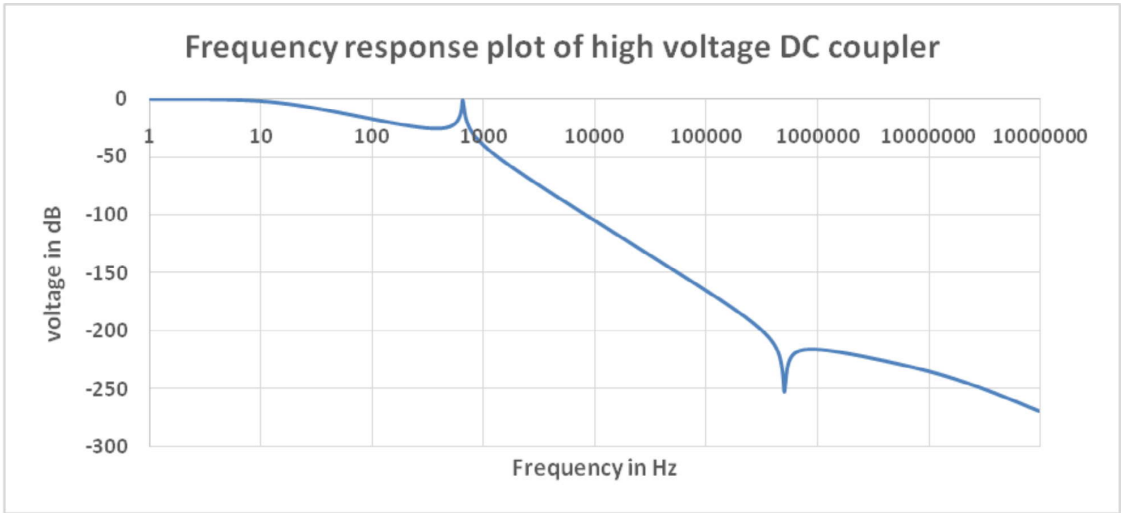

Fig. 4: High voltage DC coupler Frequency response

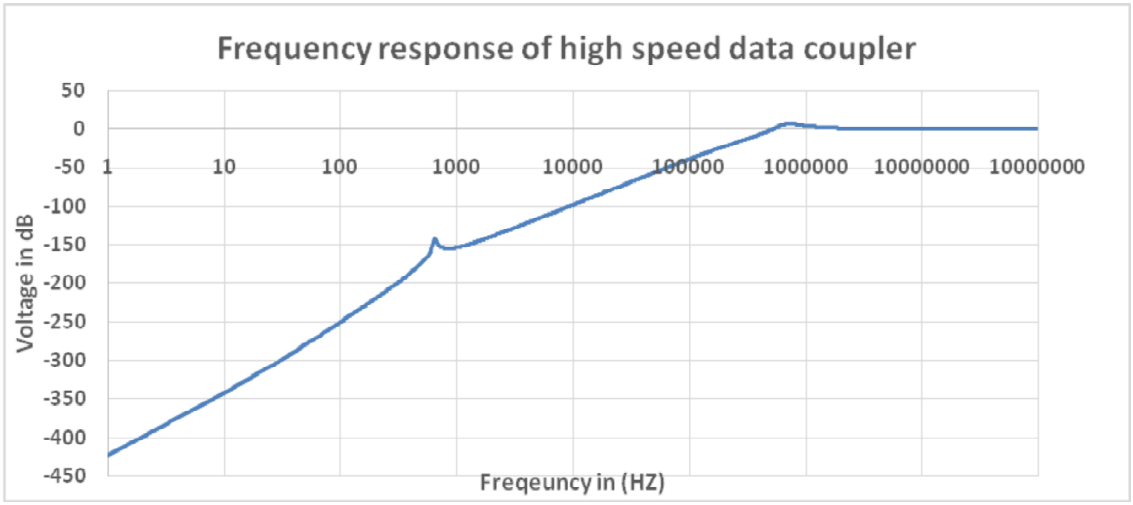

Fig. 5: Data coupler frequency response

4.2 Frequency spectrum analysis using FFT

4.2.1 Without Cable model

Simulations were carried out to find the effect of effect of cable attenuation on high voltage DC and high speed data. Time domain signals were captured while doing simulation and done the FFT analysis. Measurements were done when one input is given and all other inputs were kept as zero amplitude.

Table 1 shows the value of signals due to coupling of high voltage DC and high speed data over other coupling paths. Here the high speed data at remote data coupler attenuation is more. From the analysis, it is found that at the Onboard DC coupler, there is no component of high speed EoC data.The voltage level at the output of remote side high voltage DC coupler is 296V. The simulation without cable shows very small loss in DC voltage. There is no component of high speed data at the output of high voltage DC coupler- remote side.

Table 1: Component of signals without cable model

Coupling	DC level (dB)	DC level (V)	Data (dB)	Data (V)
Onboard Data coupler	-228	1.2nV	-0.137	9.8V
Onboard DC coupler	0	300V	-111	26µV
Remote Data coupler	-228	1.2nV	0	10V
Remote DC coupler	-0.110	296V	-111	28 µV

4.2.2 With Cable model

Table 2 shows the value of signals due to coupling of high voltage DC and high speed data over other coupling paths. Onboard DC coupler input doesn't have any high speed data component. The amplitude of the high voltage DC at the output of onboard data coupler is -228dB and that of remote coupler is -230dB. The high speed EoC data at onboard data coupler output is 2.57mV. The high voltage DC at the output of remote data coupler is 225V.

Table 2: Component of signals with cable model

Coupling	DC level (dB)	DC level (V)	Data (dB)	Data (V)
Onboard Data coupler	-228	1.18nV	-101	2.57mV
Onboard DC coupler	0	300V	-212	6.68nV
Remote Data coupler	-230	880pV	0	10V
Remote DC coupler	-2.49	225V	-111	795µV

5. MEASUREMENT AND ANALYSIS USING PROTOTYPE CIRCUIT

Based on the simulation, a prototype coupler board was developed and tested. The setups for the measurements are shown in Fig. 6. For proving the single core coaxial cable telemetry using EoC data

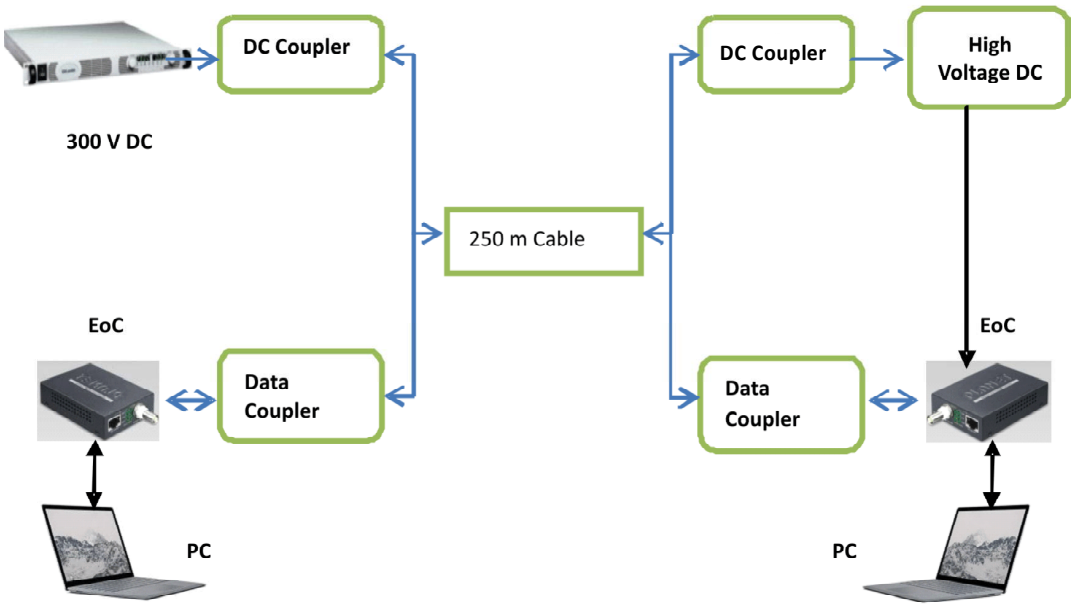

Fig. 6: Test setup for EoC Telemetry over high voltage DC

over high voltage DC needs the following setups. At onboard unit, the Ethernet data from a Personal Computer (PC) is connected to the EoC. The output of EoC is connected to the single core coaxial cable through data coupler. Similarly at the remote side, the coaxial cable data is connected to the EoC using data coupler which will convert coaxial data to Ethernet data. So EoC can be used as standard telemetry for proving the coupling schemes for single core coaxial cable telemetry.

The EoC data is connected to the single core coaxial cable is realized through high frequency data coupler. The high voltage DC should be available at remote unit throughout the operation.

Table 3 below shows the component of DC at all the coupler output. From the measurement, it is clear that there is no DC component at the output of onboard and remote high speed data coupler. Also, the DC signal gets attenuated due to the introduction of cable. At the remote side, the DC value is dropped to 220V.

Table. 3: DC signal level measurement with prototype circuit

Coupling	Data (V)
Onboard Data coupler	~0V
Onboard DC coupler	300V
Remote Data coupler	~0V
Remote DC coupler	220V

High speed data transmission from onboard unit to remote unit and remote unit to onboard unit is also verified. For this a Labview code was developed for UDP data transmission and reception. Two PCs are placed on both on-board as well as remote side. Data is successfully transmitted across the cable from onboard unit to remote unit and vice versa. The Fig. 7 shows the snapshot of the Labview GUI for data transmission and reception. Fig. 7a is the GUI for sending the control packet to remote unit.

Fig. 7b depicts the data that is transmitted from remote side PC to onboard unit. 24 channel data of sine wave with two different frequency transmitted from the remote side PC. The control data transmitted to remote unit is received and send it back to onboard along with the 24 channel sine wave data. The data transmission is also verified by connecting intranet at onboard EoC unit and Ethernet port of remote unit EoC is connected to PC. Data downloading and uploading was successfully checked.

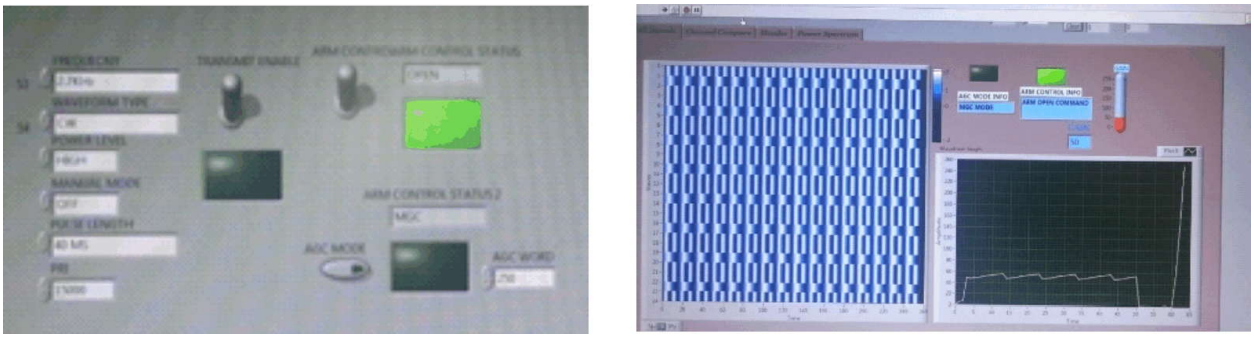

Fig. 7: Labview GUI for testing the EoC Telemetry (a) is the control GUI (b) is received packet.

6. SUMMARY AND CONCLUSIONS

EoC is a suitable standard telemetry that can be useful for single core coaxial cable telemetry. In this paper, we discussed the types of signals that are to be transmitted over single core coaxial cable and carried

out the simulation study to develop a mixing scheme to test the EoC data over single core coaxial cable. From the above simulation it is clear that the two signals like high voltage DC and high speed EoC data are able to superimpose using passive coupling scheme at one side and are able to retrieve it back using the same coupler at remote side. The transmitted signals introduce some losses due to coupling circuits and cable attenuation. The EoC module used Wideband OFDM with state of art LDPC error correction algorithm and it will automatically set for cable length up to 500m. The telemetry was tested with the new prototype board developed with high voltage 300V DC and EoC data. The data given to input of EoC is in Ethernet format at the onboard unit. The EoC at onboard unit converts the Ethernet to coaxial data. The EoC module at the remote unit converts the coaxial data back to Ethernet form. Telemetry with EoC over high voltage DC is tested and validated.

7. ACKNOWLEDGEMENT

We would like to thank Mr. S Vijayan Pillai, Director, NPOL for giving us the opportunity to carry out the work at NPOL. We also thank Mr. P Krishnakumar and Mr. P Lintish for the guidance towards completing the work.

8. REFERENCES

[1] J.E. Hardiman, T.N. Rosario, T. Quellette and F. Hegg, 2002. High repetition rate side looking SONAR. *OCEANS*'02, **4**, 2268-2272. doi: 10.1109/OCEANS.2002. 1191983

[2] E. Belcher; W. Hanot and J. Burch, 2002. Dual-frequency identification sonar (DIDSON) *International Symposium on Underwater Technology,* pp. 187-192. doi: 10.1109/UT.2002.1002424

[3] G. Manoj, E. Jacob and S.O. Kundukulam, 2016. Design, simulation and comparison of mixing schemes for DC, AC and bi-directional data through coaxial cable, *Procedia Computer Science,* pp. 578-584. doi:10.1016/j.procs.2016.07.303

[4] G. Manoj, E. Jacob and S.O. Kundukulam, 2018. Relay-based Coupling Scheme of High Speed Communication Data, High Voltage DC and High Power Pulsed AC for Coaxial Cable, *Defence Science Journal,* pp. 487-493. doi : 10.14429/dsj.68.11907

[5] M.P. Sibanda, P.A.J. van, Rensburg and H.C. Ferreira, 2013. A compact economical PLC band-pass coupler with impedance matching, *International Symposium on Power Line Communications and Its Applications (ISPLC),* pp. 339-344. doi: 10.1109/ISPLC.2013.6525874

[6] A.P. Shefter, 1993. ROV and remote data gathering control, communications, and power sup-ply over a single inexpensive coaxial cable using a low power multiplex system, *OCEANS'93 engineering in Harmony with Ocean,* **3**, pp. III/236-III/241. doi:10.1109/OCEANS.1993.326193

[7] P. Morash, C. Wortley and R. Trider, 1971. A high speed digital data system for underwater acoustic measurements, *IEEE Conference on Engineering in the Ocean Environment*, pp. 377-380. doi: 10.1109/OCEANS.1971.1161008

INFORMATION FOR AUTHORS

ARTICLES

The Journal of Acoustical Society of India (JASI) is a refereed publication published quarterly by the Acoustical Society of India (ASI). JASI includes refereed articles, technical notes, letters-to-the-editor, book review and announcements of general interest to readers.

Articles may be theoretical or experimental in nature. But those which combine theoretical and experimental approaches to solve acoustics problems are particularly welcome. Technical notes, letters-to-the-editor and announcements may also be submitted. Articles must not have been published previously in other engineering or scientific journals. Articles in the following are particularly encouraged: applied acoustics, acoustical materials, active noise & vibration control, bioacoustics, communication acoustics including speech, computational acoustics, electro-acoustics and audio engineering, environmental acoustics, musical acoustics, non-linear acoustics, noise, physical acoustics, physiological and psychological acoustics, quieter technologies, room and building acoustics, structural acoustics and vibration, ultrasonics, underwater acoustics.

Authors whose articles are accepted for publication must transfer copyright of their articles to the ASI. This transfer involves publication only and does not in any way alter the author's traditional right regarding his/her articles.

PREPARATION OF MANUSCRIPTS

All manuscripts are refereed by at least two referees and are reviewed by the Publication Committee (all editors) before acceptance. Manuscripts of articles and technical notes should be submitted for review electronically to the Chief Editor by e-mail or by express mail on a disc. JASI maintains a high standard in the reviewing process and only accept papers of high quality. On acceptance, revised articles of all authors should be submitted to the Chief Editor by e-mail or by express mail.

Text of the manuscript should be double-spaced on A4 size paper, subdivided by main headings-typed in upper and lower case flush centre, with one line of space above and below and sub-headings within a section-typed in upper and lower case understood, flush left, followed by a period. Sub-sub headings should be italic. Articles should be written so that readers in different fields of acoustics can understand them easily. Manuscripts are only published if not normally exceeding twenty double-spaced text pages. If figures and illustrations are included then normally they should be restricted to no more than twelve-fifteen.

The first page of manuscripts should include on separate lines, the title of article, the names, of authors, affiliations and mailing addresses of authors in upper and lowers case. Do not include the author's title, position or degrees. Give an adequate post office address including pin or other postal code and the name of the city. An abstract of not more than 200 words should be included with each article. References should be numbered consecutively throughout the article with the number appearing as a superscript at the end of the sentence unless such placement causes ambiguity. The references should be grouped together, double spaced at the end of the article on a separate page. Footnotes are discouraged. Abbreviations and special terms must be defined if used.

EQUATIONS

Mathematical expressions should be typewritten as completely as possible. Equation should be numbered consecutively throughout the body of the article at the right hand margin in parentheses. Use letters and numbers for any equations in an appendix: Appendix A: (A1, (A2), etc. Equation numbers in the running text should be enclosed in parentheses, i.e., Eq. (1), Eqs. (1a) and (2a). Figures should be referred to as Fig. 1, Fig. 2, etc. Reference to table is in full: Table 1, Table 2, etc. Metric units should be used: the preferred from of metric unit is the System International (SI).

REFERENCES

The order and style of information differs slightly between periodical and book references and between published and unpublished references, depending on the available publication entries. A few examples are shown below.

Periodicals:

[1] S.R. Pride and M.W. Haartsen, 1996. Electroseismic wave properties, *J. Acoust. Soc. Am.*, **100** (3), 1301-1315.

[2] S.-H. Kim and I. Lee, 1996. Aeroelastic analysis of a flexible airfoil with free play non-linearity, *J. Sound Vib.*, **193** (4), 823-846.

Books:

[1] E.S. Skudzryk, 1968. *Simple and Comlex Vibratory Systems*, the Pennsylvania State University Press, London.

[2] E.H. Dowell, 1975. *Aeroelasticity of plates and shells*, Nordhoff, Leyden.

Others:

[1] J.N. Yang and A. Akbarpour, 1987. Technical Report NCEER-87-0007, Instantaneous Optimal Control Law For Tall Buildings Under Seismic Excitations.

SUMISSIONS

All materials from authors should be submitted in electronic form to the JASI Chief Editor: B. Chakraborty, CSIR - National Institute of Oceanography, Dona Paula, Goa-403 004, Tel: +91.832.2450.318, Fax: +91.832.2450.602,(e-mail: bishwajit@nio.org) For the item to be published in a given issue of a journal, the manuscript must reach the Chief Editor at least twelve week before the publication date.

SUMISSION OF ACCEPTED MANUSCRIPT

On acceptance, revised articles should be submitted in electronic form to the JASI Chief Editor (bishwajit@nio.org)